2018

Single-cell RNA-seq uncovers a robust transcriptional response to morphine by glia

Denis Avey
Washington University School of Medicine in St. Louis

Sumithra Sankararaman
Washington University School of Medicine in St. Louis

Aldrin K.Y. Yim
Washington University School of Medicine in St. Louis

Ruteja Barve
Washington University School of Medicine in St. Louis

Jeffrey Milbrandt
Washington University School of Medicine in St. Louis

See next page for additional authors

Resource

Cell Reports

Single-Cell RNA-Seq Uncovers a Robust Transcriptional Response to Morphine by Glia

Graphical Abstract

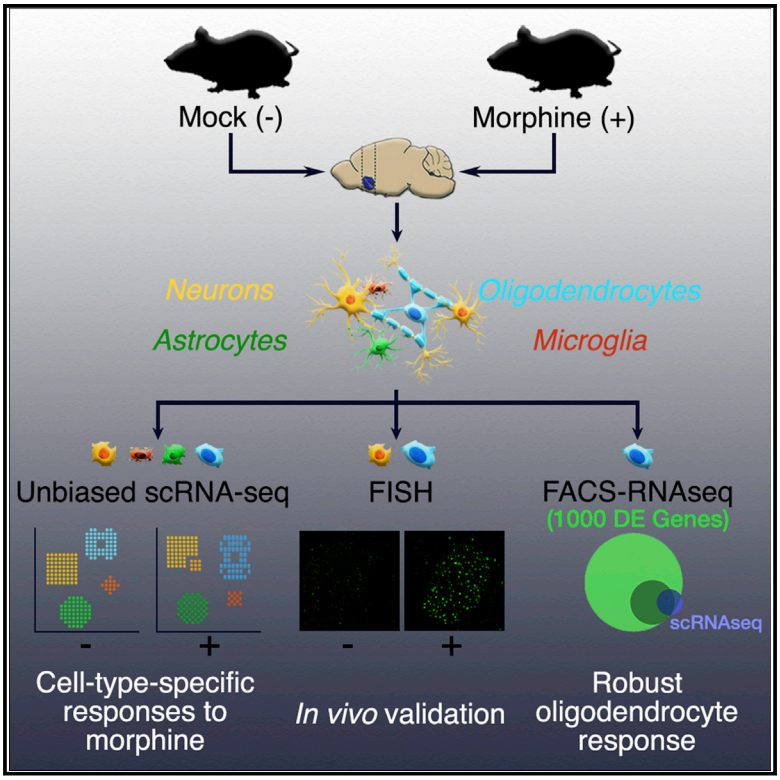

Highlights

- Single-cell RNA-seq uncovers cell-type-specific responses to morphine in mice
- Among glia, the most robust transcriptional response are in oligodendrocytes
- Oligodendrocyte- and neuron-specific responses to morphine are validated by FISH
- Bulk RNA-seq of purified oligodendrocytes reveals ~1,000 morphine-regulated genes

Authors

Denis Avey, Sumithra Sankararaman, Aldrin K.Y. Yim, Ruteja Barve, Jeffrey Milbrandt, Robi D. Mitra

Correspondence

jmilbrandt@wustl.edu (J.M.), rmitra@wustl.edu (R.D.M.)

In Brief

Avey et al. use single-cell RNA-seq to uncover cell-type-specific responses to morphine in the brains of mice, revealing a unique and robust response by oligodendrocytes, which they further validate by multiple approaches. These analyses offer insights into the molecular mechanisms underlying oligodendrocyte dysfunction in the context of opioid abuse.

Avey et al., 2018, Cell Reports *24*, 3619–3629
September 25, 2018
https://doi.org/10.1016/j.celrep.2018.08.080

CellPress

Cell Reports
Resource

Single-Cell RNA-Seq Uncovers a Robust Transcriptional Response to Morphine by Glia

Denis Avey,[1,2] Sumithra Sankararaman,[2] Aldrin K.Y. Yim,[1] Ruteja Barve,[3] Jeffrey Milbrandt,[1,*] and Robi D. Mitra[1,2,4,*]
[1]Department of Genetics, Washington University, School of Medicine, St. Louis, MO 63110, USA
[2]Center for Genome Sciences and Systems Biology, Washington University, School of Medicine, St. Louis, MO 63110, USA
[3]Genome Technology Access Center, Department of Genetics. Washington University, School of Medicine, St. Louis, MO 63110, USA
[4]Lead Contact
*Correspondence: jmilbrandt@wustl.edu (J.M.), rmitra@wustl.edu (R.D.M.)
https://doi.org/10.1016/j.celrep.2018.08.080

SUMMARY

Molecular and behavioral responses to opioids are thought to be primarily mediated by neurons, although there is accumulating evidence that other cell types play a prominent role in drug addiction. To investigate cell-type-specific opioid responses, we performed single-cell RNA sequencing (scRNA-seq) of the nucleus accumbens of mice following acute morphine treatment. Differential expression analysis uncovered unique morphine-dependent transcriptional responses by oligodendrocytes and astrocytes. We examined the expression of selected genes, including *Cdkn1a* and *Sgk1*, by FISH, confirming their induction by morphine in oligodendrocytes. Further analysis using RNA-seq of FACS-purified oligodendrocytes revealed a large cohort of morphine-regulated genes. The affected genes are enriched for roles in cellular pathways intimately linked to oligodendrocyte maturation and myelination, including the unfolded protein response. Altogether, our data illuminate the morphine-dependent transcriptional response by oligodendrocytes and offer mechanistic insights into myelination defects associated with opioid abuse.

INTRODUCTION

Drug addiction is a global health concern associated with considerable adverse impacts. Affected individuals experience severe physical and emotional hardship, which also takes a toll on their families and society (Bauer et al., 2015; Dart et al., 2015). The fiscal consequences in the United States alone have been estimated to exceed $600 billion a year (https://www.drugabuse.gov/publications/principles-drug-addiction-treatment-research-based-guide-third-edition/preface). The current epidemic of prescription opioid abuse has contributed to an alarming rise in overdose death rates (Dart et al., 2015). Opioid-dependent individuals also exhibit increased comorbidity with other psychiatric disorders, including depression, as well as impaired white matter integrity and consequent cognitive deficits (Bora et al., 2012; Liu et al., 2008). Although environmental risk factors contribute to drug addiction, it is well-established that acute drug exposure induces gene expression changes in the CNS and that these changes affect susceptibility to addiction (Lüscher and Malenka, 2011).

All addictive drugs modulate the mesolimbic pathway of the brain by elevating dopamine levels in the nucleus accumbens (NAc), a region in the ventral striatum with a central role in processing motivation, reward, aversion, and reinforcement learning (Volkow and Morales, 2015). Because of this, researchers have aimed to elucidate the effects of various addictive drugs, including methamphetamine (Piechota et al., 2010; Zhu et al., 2015), cocaine (Albertson et al., 2006; Piechota et al., 2010), and opioids (Albertson et al., 2006; Korostynski et al., 2007; Piechota et al., 2010), on gene expression in the NAc. However, because the brain is an exceptionally heterogeneous tissue, previous experiments using bulk tissue preparations could not confidently ascribe gene expression changes to a certain cell type, thereby precluding the elucidation of cellular and molecular mechanisms of drug abuse. Advances in microfluidics and sequencing technology make it feasible to analyze thousands of single-cell transcriptomes in a single experiment. Various single-cell RNA sequencing (scRNA-seq) platforms have been developed (Cao et al., 2017; Islam et al., 2014; Klein et al., 2015; Zheng et al., 2017), enabling the characterization of dozens of molecularly distinct CNS cell types from multiple regions.

We profiled the gene expression of 23,276 individual cells from the NAc of mice using Drop-seq (Macosko et al., 2015). Differential expression analysis uncovered numerous cell-type-specific changes in gene expression due to acute morphine treatment. We observed a dramatic morphine-dependent transcriptional response in oligodendrocytes, which was an unorthodox result given that no study has described opioid-dependent gene expression changes unique to oligodendrocytes. We validated the morphine-dependent and cell-type-specific expression of a subset of genes by using fluorescence *in situ* hybridization (FISH). We also performed bulk RNA sequencing (RNA-seq) of oligodendrocytes isolated from mock- or morphine-treated mice, which confirmed a robust transcriptional response to morphine in these cells. We identified key molecular pathways modulated by morphine in oligodendrocytes that are likely to underlie the myelination defects associated with heroin abuse in human patients.

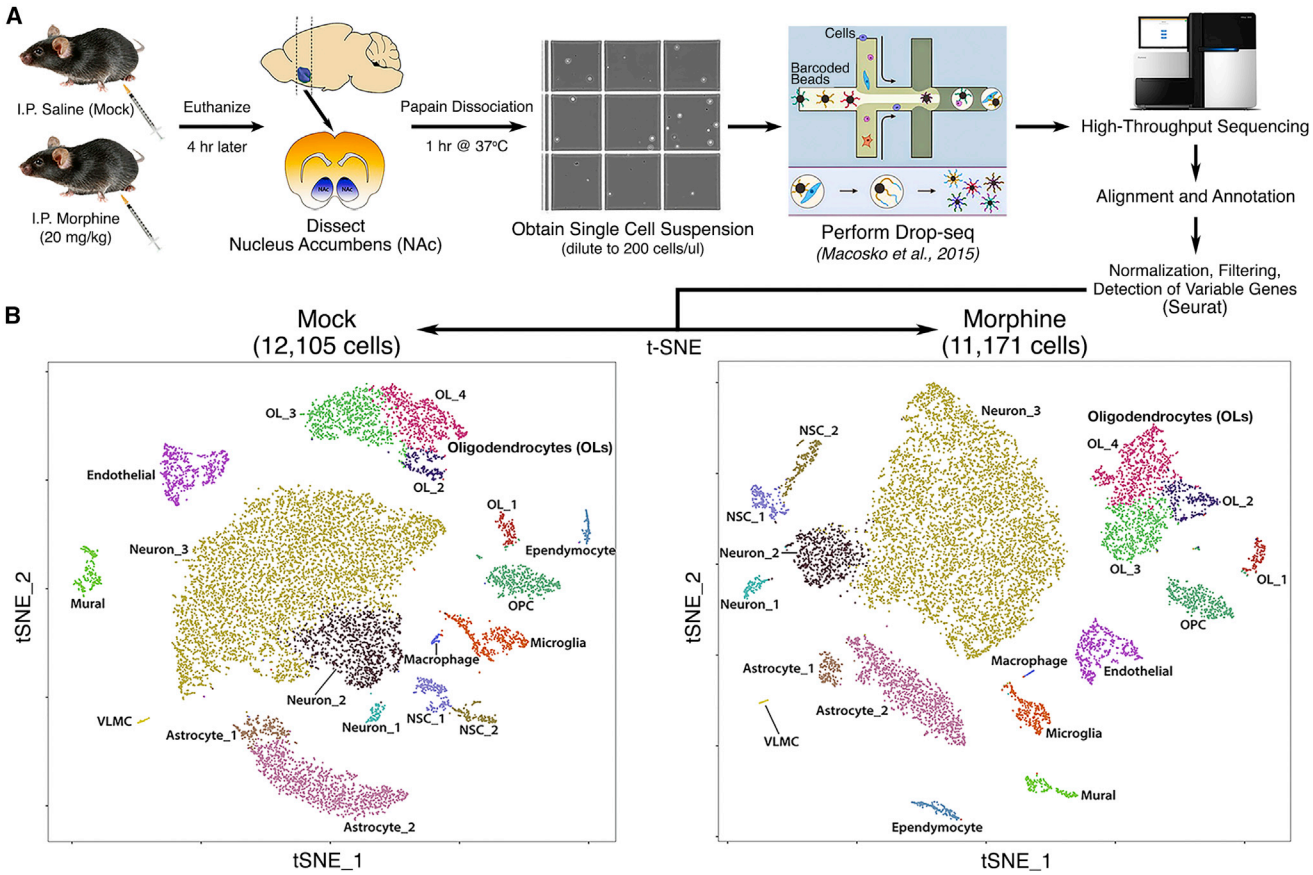

Figure 1. Unbiased Single-Cell RNA-Seq Analysis Identified 18 Distinct Cell Types in the Nucleus Accumbens of Mice

(A) Flowchart showing an overview of the single-cell RNA-seq experimental design.

(B) Spectral t-SNE plots of all cells analyzed from mock-treated mice (12,105) or morphine-treated mice (11,171), colored by density clustering and annotated by cell-type identity. OPC, oligodendrocyte progenitor cell; NSC, neural stem cell; VLMC, vascular and leptomeningeal cell.

RESULTS

Unbiased scRNA-Seq Analysis Identified 18 Distinct Cell Types in the NAc of Mice

The molecular responses to morphine and other drugs of abuse by the neurons of the NAc have been well studied. However, the responses by specific neuronal or glial subpopulations have not been investigated in an unbiased and high-throughput manner. To address this, we treated mice with morphine or saline as a mock control and 4 hr later dissected the NAc. We chose 4 hr because it is the time at which the maximal number and magnitude of gene expression changes were observed in previous studies of the striatal transcriptional response to morphine (Korostynski et al., 2007; Piechota et al., 2010). A single-cell suspension was prepared from the dissociated tissue, and Drop-seq (Macosko et al., 2015) was used to obtain transcriptomes from 23,276 single cells (Figure 1A). We sequenced these cells to an average depth of ~67,000 reads/cell and detected 1,612 mean genes and 3,228 mean transcripts (Figure S1). Using principal-component analysis (PCA), graph-based clustering, and dimensionality reduction for 2D visualization through t-distributed stochastic neighbor embedding (t-SNE) (van der Maaten, 2008), we identified 18 distinct clusters (Figure 1B), all of which were present at nearly identical ratios in mock- and morphine-treated mice and at comparable ratios among biological replicates (Table S1). Next, we assigned a major CNS cell-type identity to each cluster (Figure 1B) by cross-referencing genes that were enriched in specific clusters with published gene expression datasets (Gokce et al., 2016; Zhang et al., 2014). Many cluster-enriched genes have been previously identified as markers for specific cell types (Table S1), and the overall gene expression profiles of our samples correlate well with bulk RNA-seq (Hodes et al., 2015) or scRNA-seq (Gokce et al., 2016) analyses of the striatum (Figure S1). Clusters from mock- and morphine-treated mice exhibited striking similarities in cell number, number of genes detected per cell, and expression levels of cluster-enriched genes (Figure S2), indicating that the overall cell-type composition of the NAc is unchanged by acute morphine treatment.

Subclustering of Neurons Enables the Identification of a Subpopulation of Morphine-Activated MSNs

The NAc is composed of many neuronal subtypes, yet our initial t-SNE analysis resolved only three neuronal clusters. To increase

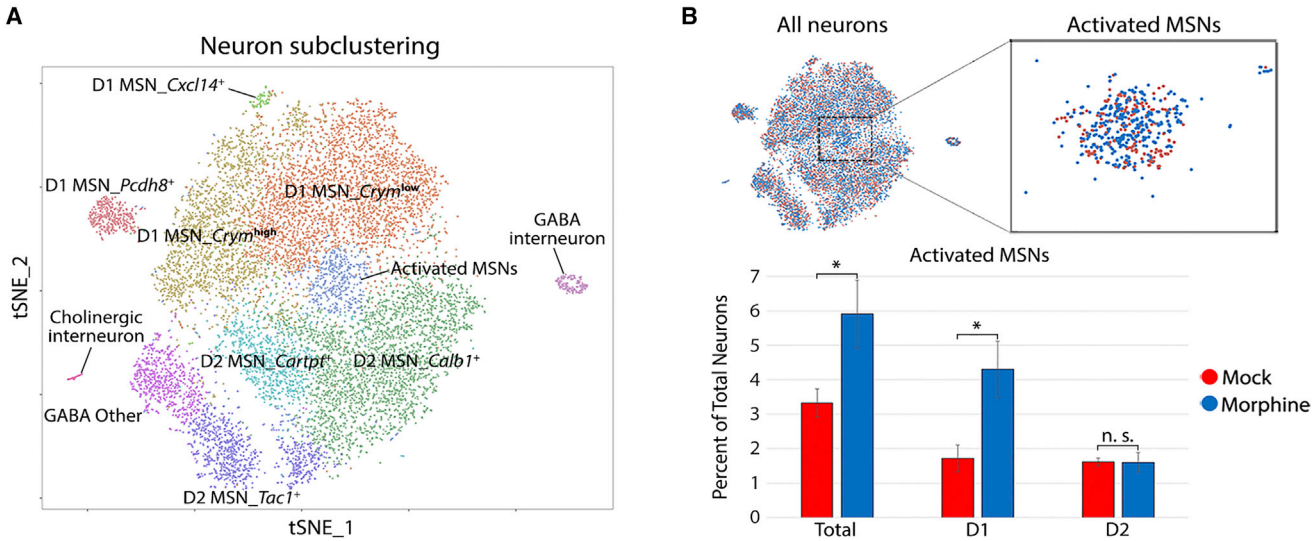

Figure 2. Iterative Clustering of Neurons Enables the Identification of a Subpopulation of Morphine-Activated MSNs

(A) Spectral t-SNE plot of 13,033 neurons, annotated by cell-type identity. MSN, medium spiny neuron.

(B) Zoomed view of all-neuron t-SNE with cells colored by treatment. Bar graph displays the percentage of total neurons in the activated MSN cluster, stratified by treatment and expression of the dopamine receptor (D1 versus D2). Error bars show SD among four biological replicates (*p = 0.028, paired t test, two-sided).

resolution, we re-clustered all cells initially identified as neurons, revealing 11 clusters (Figure 2A; Table S1). These clusters directly correspond to the previously identified neuronal subtypes of the NAc. For example, γ-aminobutyric acid-ergic (GABAergic) D1 and D2 medium spiny neurons (MSNs) are known to comprise ~95% of the neurons in the NAc (Lobo et al., 2006); accordingly, we found two major populations of neurons that were enriched for expression of either *Drd1a*, *Tac1*, and *Pdyn* (D1 MSNs) or *Drd2*, *Penk*, and *Adora2a* (D2 MSNs) (Figure S3; Table S1). Another ~2% of the neurons we identified were GABAergic (*Sst*$^+$/*Npy*$^+$) and cholinergic (*Chat*$^+$/*Slc5a7*$^+$) interneurons. The ubiquitous expression of *Gad2* (GABA neuron marker) and *Ppp1r1b* (striatal neuron marker) and sparse detection of the glutamate neuron-specific gene *Slc17a7* indicate that our dissections of the NAc were highly accurate, containing minimal contamination with adjacent tissues such as the cortex (Figure S3). Overall, the neuronal subtype diversity that we uncovered is highly concordant with previous studies of cellular diversity in the NAc, including a previously described single-cell analysis of the striatum (Gokce et al., 2016).

We were intrigued by a cluster of neurons in the center of the t-SNE plot characterized by high expression of several immediate early genes (IEGs), such as *Fos* (*c-fos*), *Junb*, *Arc*, and *Nr4a1* (Figure 2; Figure S3). Morphine treatment resulted in a statistically significant two-fold increase in the proportion of these activated MSNs (Figure 2B). It has been reported that *c-fos* protein expression is upregulated specifically in D1 MSNs upon acute morphine treatment (Enoksson et al., 2012). Consistent with this, *Drd1a*-expressing cells account for the morphine-dependent increase in the proportion of activated MSNs (Figure 2B). Furthermore, gene set enrichment analysis indicated that genes enriched in this cluster are associated with several terms related to opioid addiction, including morphine dependence and opioid-related disorders (Table S3). Thus, we identified a subpopulation of neurons displaying a canonical transcriptional response to acute morphine treatment.

Cell-Type-Specific Differential Expression Analysis Uncovered a Robust Morphine-Dependent Transcriptional Response in Oligodendrocytes

The primary goal of this study was to identify cell-type-specific alterations in gene expression induced by morphine. To accomplish this, we used single-cell differential expression (SCDE) software that uses a Bayesian approach to detect differentially expressed (DE) genes from single-cell data (Kharchenko et al., 2014). We presumed that MSNs would exhibit the strongest transcriptional response, because these cells are known to express opioid receptors, display an electrophysiological response to morphine, and mediate morphine-induced behavioral phenotypes. We found that morphine induces the expression of several hundred genes, including the classical markers *Fos*, *Junb*, and *Nr4a1*, in D1 neurons of the activated MSN cluster compared to other D1 neurons (Table S2). We also detected morphine-dependent changes in gene expression in nearly every glial cell type, with the most numerous changes found in oligodendrocytes (OLs) (Figure 3). Morphine elicited significant alterations in gene expression in each of six clusters of OLs (Figure 3B; Figure S4), which correspond to developmental states in the continuum from oligodendrocyte progenitor cells (OPCs) to myelin-forming OLs (MFOLs) and mature OLs (MOLs) (Figure 4A) (Marques et al., 2016). Many of the morphine-induced genes identified in MFOLs and MOLs, including *Cdkn1a*, *Phactr3*, and serum/glucocorticoid-regulated kinase 1 (*Sgk1*), have been previously reported to be upregulated by morphine in the striatum (Korostynski et al., 2007; Piechota et al., 2010; Skupio et al., 2017), but these changes could not be confidently ascribed to a specific

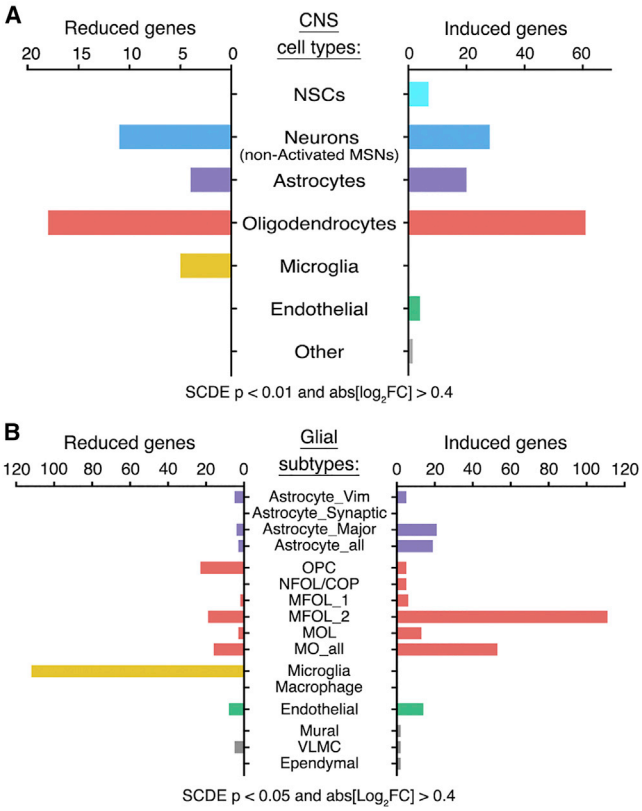

Figure 3. SCDE Analysis Uncovered Cell-Type-Specific Responses to Morphine

(A and B) We performed single-cell differential expression (SCDE) (morphine versus mock) on each t-SNE cluster. The total number of unique genes significantly induced or reduced by morphine is shown, grouped by (A) major CNS cell type or (B) glial subpopulation. Astrocyte_Vim, Astrocyte_Synaptic, and Astrocyte_Major refer to three subclusters of astrocytes, and Astrocyte_all is the combined analysis of all astrocytes. MO_all denotes the combined analysis of all MFOLs and/or mature oligodendrocytes (e.g., MFOL_1, MFOL_2, and MOL). See STAR Methods and Table S2 for additional details. Full terms for abbreviations of oligodendrocyte clusters (red) are given in the legend of Figure 4.

cell type (Figure 4B, bolded genes). 13 of the top 30 morphine-induced genes in OLs (SCDE p value < 0.0001) are reported targets of the glucocorticoid receptor (GR) (Figure 4B, marked by asterisks). GR signaling is known to play a key role in morphine-dependent gene expression and behaviors in mice (Marinelli et al., 1998) and was shown to be critical for a large subset of morphine-induced transcriptional responses in cultured astrocytes (Slezak et al., 2013). We found a significant enrichment of GR targets among morphine-induced genes in astrocytes but also uncovered a distinct subset of GR target genes in OLs (Figure 4C; Table S3). Altogether, these data suggest a robust and previously underappreciated transcriptional response to morphine in OLs. Because multiple studies suggest myelin pathology in human opioid addicts (Bora et al., 2012; Li et al., 2016; Liu et al., 2008; Upadhyay et al., 2010; Wang et al., 2011), we pursued this observation, with the goal of illuminating the molecular mechanisms by which morphine influences OL function.

In Vivo Validation of Cell-Type-Specific Morphine-Dependent Changes in Gene Expression by FISH

Although single-cell mRNA profiling is widely used for the identification of new cellular subtypes, calling DE genes from these data can be challenging due to technical issues such as dropout and dynamic range compression (Dal Molin et al., 2017). Therefore, we sought to independently validate some of the most dramatic morphine-dependent changes in gene expression. We used FISH to costain *Cdkn1a* or *Sgk1* and *Mbp* (myelin basic protein), a highly expressed marker of OLs (Figure 5A). The *Cdkn1a* and *Sgk1* signal was sparsely detected in mock-treated mice, while morphine treatment elicited a dramatic increase in puncta number selectively in OLs (Figures 5B–5D). The morphine-dependent increase was observed throughout the NAc and dorsal striatum but was especially apparent in oligodendrocyte-dense white matter tracts, such as the anterior commissure (Figure 5B) and corpus callosum (Figure 5C). This suggests that the OL response to morphine is likely not restricted to the NAc. The anterior commissure was included within our initial NAc dissections; thus, OL lineage cells from this region comprise a significant fraction of the total OLs in our scRNA-seq dataset (roughly 25% based on estimates from the *Mbp* FISH signal). When mice were pre-treated with naltrexone (NTX), an opioid receptor antagonist, the morphine-dependent induction of *Cdkn1a* and *Sgk1* was dramatically reduced (Figures 5A–5D), indicating that their induction occurs in an opioid receptor-dependent manner. As expected, morphine-dependent induction of the immediate-early genes *Fos*, *Junb*, and *Nr4a1* was observed in the NAc and dorsal striatum, predominantly in *Drd1*-expressing cells (D1 MSNs), and was similarly reduced by NTX pre-treatment (Figure S5). Altogether, these results validate the cell-type-specific transcriptional responses we identified by scRNA-seq and suggest that both neuron- and OL-specific changes are mediated by opioid receptor activation.

Bulk RNA-Seq of FACS-Isolated OLs Revealed a Remarkable Extent of Transcriptional Regulation by Morphine

Because our Drop-seq and FISH data indicated a robust oligodendrocyte transcriptional response to morphine *in vivo*, we sought to validate this finding *in vitro*. We treated purified cultures of mouse OLs with morphine and assessed expression of *Cdkn1a*, *Sgk1*, and *Phactr3* by qRT-PCR. Expression of these genes was not appreciably affected by morphine (Figure S6), suggesting that the response we observed *in vivo* might be mediated by an indirect or non-cell-autonomous mechanism. To further characterize this response, we adapted an immunostaining and fluorescence-activated cell sorting (FACS)-based approach (Robinson et al., 2014) to isolate OLs from the entire brains of six mice, three each mock or morphine treated. Saline or morphine injections and tissue dissociation were performed exactly as in our scRNA-seq experiments to enable cross-validation between the two datasets. We gated out $CD45^+$ and $PDGFRa^+$ populations to remove immune cells and OPCs, respectively, and then isolated MFOLs and/or MOLs based on their dual expression of GALC and MOG (Figure S7A). RNA was purified from each of the six samples and examined by qRT-PCR. We found 10- to 20-fold enrichment of the OL markers

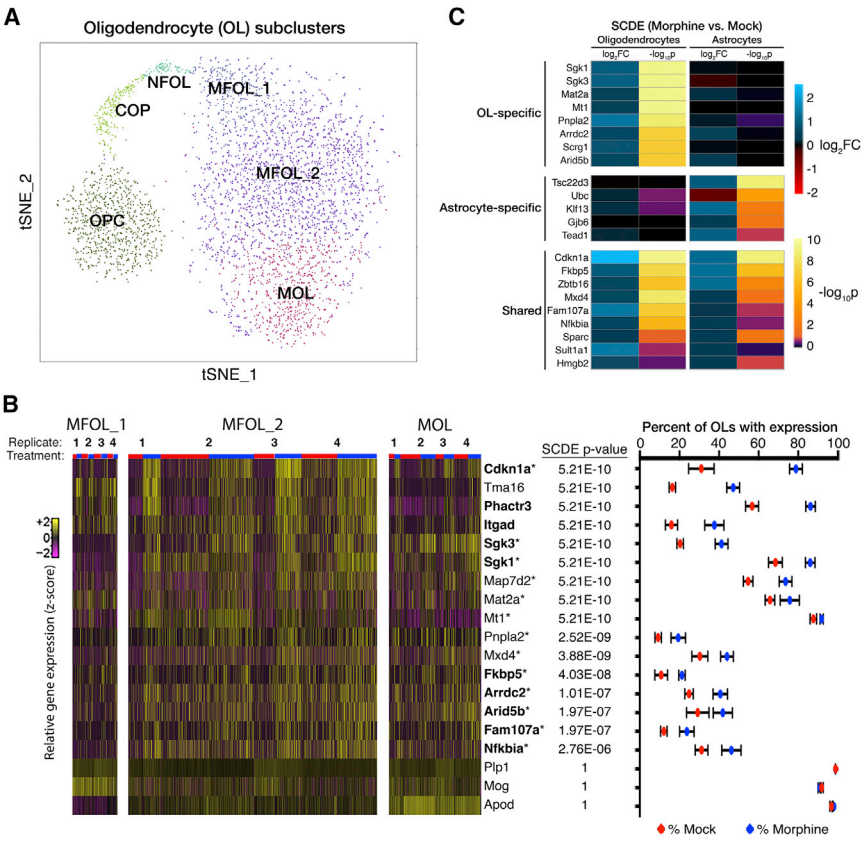

Figure 4. Iterative Clustering and SCDE Revealed a Robust Morphine-Dependent Transcriptional Response by Oligodendrocytes

(A) Iterative clustering of all 3,817 oligodendrocytes (OLs) reveals subpopulations corresponding to OL maturation state. OPC, oligodendrocyte progenitor cell; COP, differentiation-committed OL progenitor; NFOL, newly formed OL; MFOL, myelin-forming OL; MOL, mature OL.

(B) Morphine robustly modulates the expression of several genes in OLs. (Left) Heatmap of relative gene expression for a subset of genes in three clusters of MFOLs and/or mature OLs. Columns representing individual cells are ordered horizontally by biological replicate and treatment (red, mock; blue, morphine). Bolded genes have been previously reported to be induced by morphine in the mouse striatum, and those marked with an asterisk are reported targets of the glucocorticoid receptor (GR). (Right) SCDE p value and expression percentages for combined analysis of all MFOLs and/or mature OLs (MFOL_1, MFOL_2, and MOL). Expression is defined as detection of ≥1 transcript. Dots and error bars are, respectively, the mean and SD among four biological replicates.

(C) Morphine regulates the expression of distinct subsets of GR target genes in OLs and astrocytes.

Cnp and *Mog*, which was comparable to that observed following affinity purification of ribosome-associated mRNAs from Cnp-Cre x HA-Rpl22 (Ribotag) mice (Sanz et al., 2009). A significant reduction of the neuronal marker *Rbfox3/NeuN* and the astrocytic marker *Gfap* in these FACS samples indicated enhanced specificity of this approach compared to the Ribotag method (Figures S7B and S7C). Assured that this was an enriched OL population, we tested the morphine-dependent upregulation of *Cdkn1a* and *Sgk1* by qRT-PCR and found that they were induced by more than 10-fold (Figure S7C).

To ascertain the full extent of morphine-dependent transcriptional regulation in OLs, we next performed RNA-seq on these sorted samples. We reasoned that the FACS population should be most comparable to the three MFOLs and/or MOL clusters observed in our single-cell transcriptional profiling (MFOL_1, MFOL_2, and MOL), because these clusters specifically and ubiquitously express *Mog*. Differential expression analysis of the bulk FACS-RNA-seq data confirmed 85.5% (59/69) of the changes detected by single-cell analysis (SCDE) of OLs. In addition, we uncovered an additional 935 genes significantly affected by acute morphine treatment (DESeq adjusted p value [p-adj] < 0.05 and abs[$\log_2$FC] > 0.5) (Figure 6A; Table S5). These results demonstrate that most morphine-dependent expression changes detected by single-cell RNA-seq were bona fide; in addition, our bulk RNA-seq experiments identified a large set of expression changes that were not observed in our single-cell experiments, illustrating the increased sensitivity of the FACS-RNA-seq approach. Considering the FACS-RNA-seq dataset as the gold standard upon which to benchmark single-cell DE analysis, we optimized the sensitivity of single-cell DE calling by filtering out lowly expressed genes (those detected in less than 2% of cells), removing a fold-change cutoff, and relaxing the SCDE p value cutoff. These criteria effectively doubled the number of DE genes detected in MFOLs and/or MOLs without compromising specificity (Figure 6B, compare green dot and red diamond). Of the most significant morphine-regulated genes identified by a previous microarray analysis of the striatum (Piechota et al., 2010), nearly half of them can be attributed to OLs (Figure 6C). In addition, our single-cell analysis allowed us to ascribe other reported morphine-dependent gene expression changes to neurons or astrocytes (Figure 6C). A comparison of our data to changes observed at various time points following acute morphine treatment (1, 2, 4, or 8 hr) indicates cell-type-specific differences in the temporal response to morphine (Figure S8). These analyses underscore the utility of cell-type-specific profiling strategies and suggest that oligodendrocyte-specific responses to opioids have been underappreciated.

To obtain biological insights into the response to morphine by OLs, we performed gene set enrichment and pathway analyses of our FACS-RNA-seq data. This confirmed the enrichment of GR targets, including all GR-related genes we identified by Drop-seq, among the morphine-induced genes in OLs (Figure S9; Table S3). We also found that several morphine-repressed genes encode endoplasmic reticulum (ER) chaperone proteins with critical functions in ER quality control (ERQC) and

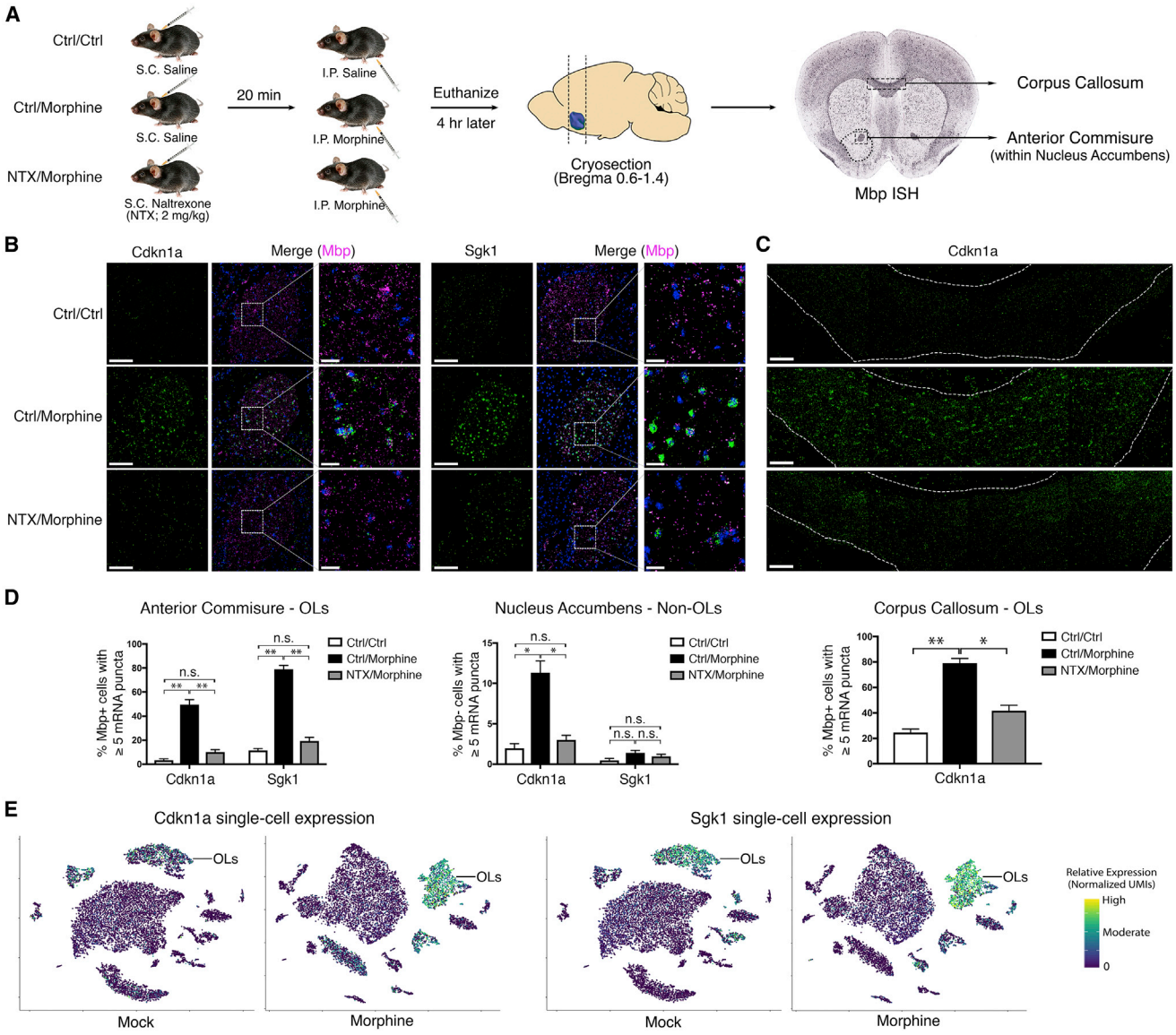

Figure 5. *In Vivo* Validation of Oligodendrocyte-Specific Morphine-Dependent Gene Expression by FISH

(A) Schematic of experimental design. Pre-treatment with naltrexone (NTX) should block morphine responses mediated by opioid receptor activation. *Mbp in situ* hybridization (ISH) (from the Allen Brain Atlas database) is shown to illustrate regions with high densities of OLs.

(B and C) Expression of *Cdkn1a* and *Sgk1* is induced by morphine in OLs in an opioid receptor-dependent manner. Representative images of the anterior commissure (B) and corpus callosum (C) are shown. Signals are pseudocolored by expression of *Cdkn1a* (green), *Sgk1* (green), *Mbp* (magenta), and/or DAPI (blue). Scale bars, 100 μm (left panels) and 20 μm (right panels and zoomed view).

(D) Quantification of the percentage of OLs (left panel: n = 781 cells; right panel: n = 1,374 cells) or of non-OLs (middle panel: n = 1,000 cells) with ≥5 puncta of *Cdkn1a* or *Sgk1* (3 mice per condition; paired t test, two-sided; NS, not significant; $^{**}p < 1e{-}4$, $^{*}p < 0.05$).

(E) t-SNE plots of all cells from mock- or morphine-treated mice overlaid with expression of *Cdkn1a* or *Sgk1* indicates that the morphine-dependent induction of these genes occurs predominantly in OLs. In the case of *Cdkn1a*, a modest induction was also detected in astrocytes and endothelial cells.

the unfolded protein response (UPR) (Figure 7; Figure S9). MFOLs are thought to be particularly susceptible to ER stress because of their high rates of protein and lipid synthesis (Lin and Popko, 2009). Accordingly, components of the UPR machinery are dysregulated in various demyelinating diseases of the peripheral and CNS (Lin and Popko, 2009). The morphine-dependent downregulation of ERQC and UPR could lead to an increase in the intracellular accumulation and/or export of misfolded proteins, as well as downstream consequences on oligodendrocyte survival, maturation, and/or myelination. This has considerable clinical implications in light of several studies describing impaired white matter integrity in the brains of human opioid users (Bora et al., 2012; Li et al., 2016; Liu et al., 2008; Upadhyay et al., 2010; Wang et al., 2011).

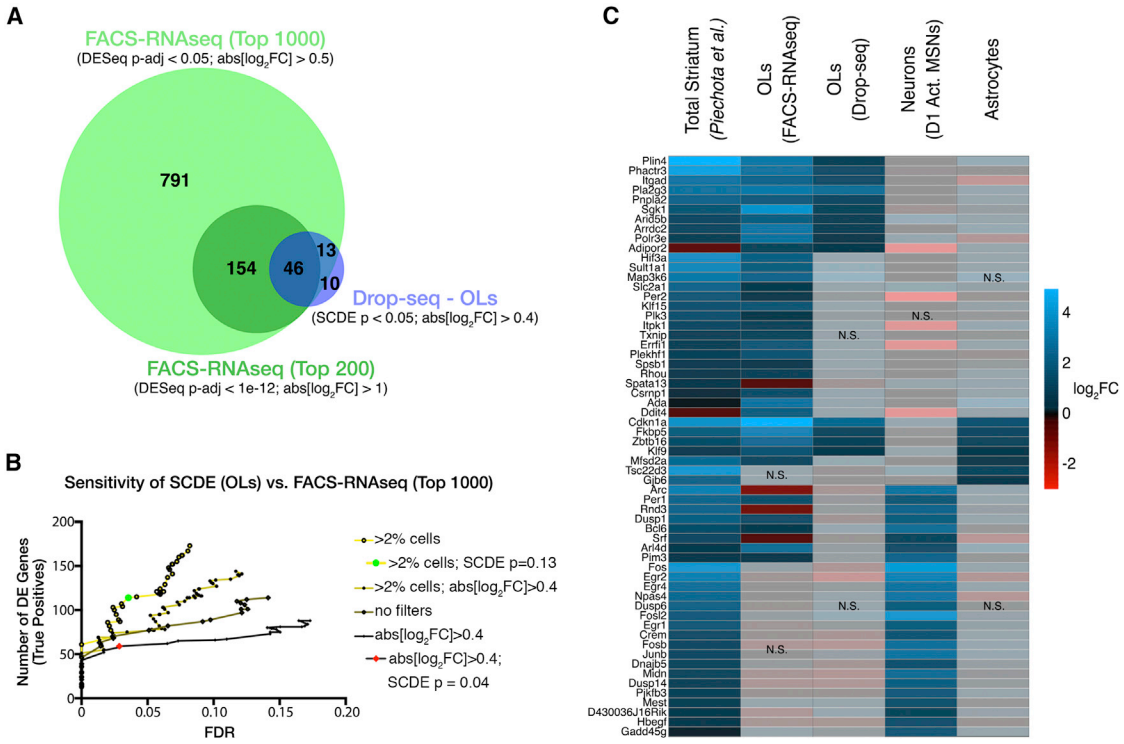

Figure 6. Bulk RNA-Seq of FACS-Isolated OLs Revealed a Remarkable Extent of Transcriptional Regulation by Morphine

(A) Venn diagram illustrating significant overlap between DE genes identified from Drop-seq (OLs) or FACS-RNA-seq.

(B) We improved the sensitivity of single-cell DE analysis with minimal loss in specificity. The number of DE genes (true positives: present in the FACS-RNA-seq top 1,000 list) detected by SCDE of OLs was plotted versus the empirical false discovery rate (FDR; STAR Methods). We optimized SCDE by filtering out genes expressed in less than 2% of cells, removing a fold-change cutoff, and relaxing the p value cutoff to 0.13 (green circle).

(C) Left column of the heatmap shows the relative morphine-dependent induction (log_2FC morphine versus saline: 4 hr) of a subset of genes previously reported to be induced by morphine, as assessed by microarray of total striatum (Piechota et al., 2010). We filtered the top 100 morphine-regulated genes from that dataset for those significantly affected in OLs (FACS-RNA-seq and/or Drop-seq), *Drd1a*-expressing activated MSNs (D1 Act. MSNs), or astrocytes to obtain the 60 genes shown here. Opaque blocks (labeled NS) indicate changes that were not statistically significant ($p < 0.05$).

DISCUSSION

Molecular and behavioral responses to opioids have long been presumed to be mediated by neurons. The finding that OLs and astrocytes express opioid receptors *in vitro* and *in vivo* suggested that they too might respond to opioids (Knapp et al., 1998; Stiene-Martin et al., 2001). Astrocyte proliferation is reduced by stimulation of mu opioid receptor (MOR), kappa opioid receptor (KOR), or delta opioid receptor (DOR) (Stiene-Martin and Hauser, 1991; Hauser et al., 1996) and morphine-induced transcriptional responses of primary astrocytes have been described (Slezak et al., 2013). MOR agonists enhance proliferation of immature OLs, but not MOLs (Knapp and Hauser, 1996), while KOR agonists appear to promote OL differentiation and myelination (Knapp et al., 1998; Mei et al., 2016; Du et al., 2016). Altogether, previous reports indicate that opioids differentially influence the survival, proliferation, and/or differentiation of OLs and astrocytes, but the molecular mechanisms remain poorly understood. Brain imaging of heroin users has revealed impaired white matter integrity, implicating OLs in the pathophysiology of opioid dependence (Bora et al., 2012; Li et al., 2016; Liu et al., 2008; Upadhyay et al., 2010; Wang et al., 2011). Heroin abuse has also been linked to leukoencephalopathies that are likely mediated by OL dysfunction (Bach et al., 2012). We performed unbiased profiling of cell-type-specific transcriptional responses to morphine and uncovered a remarkable number of alterations in gene expression that are unique to OLs. Many of the gene expression changes we observed in OLs are also altered following chronic opioid morphine exposure (Skupio et al., 2017). Our results are consistent with previous reports suggesting a role for opioid signaling in OL maturation and myelination. Moreover, our detailed characterization of the OL-specific response to morphine offers insights into the putative mechanisms of OL dysfunction in opioid-induced myelin pathology.

The most significantly DE gene we detected in OLs is *Cdkn1a*, which encodes p21. The major function of p21 is the inhibition of cyclin-dependent kinases that leads to cell-cycle arrest. In OLs, its expression is required for differentiation and myelination (Zezula et al., 2001). It has been demonstrated that autonomous transforming growth factor β (TGF-β) signaling drives oligodendrocyte differentiation and CNS myelination during postnatal development via SMAD3/4-dependent transcriptional activation of *Cdkn1a* and repression of *Myc* (*c-myc*) (Palazuelos et al., 2014). We observed morphine-dependent reduction in the

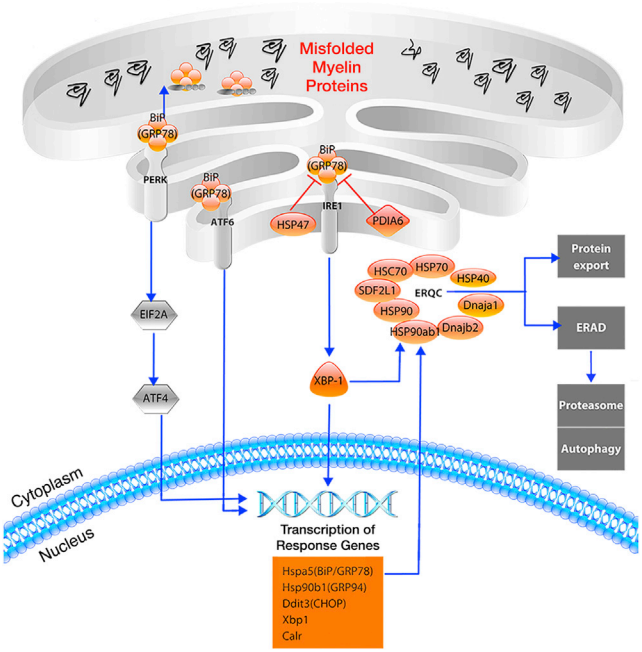

Figure 7. Several Components of the UPR Are Downregulated by Morphine in OLs

Genes downregulated by morphine in OLs (p-adj < 1e−8, $\log_2$FC < −0.5) are shown in orange, and unaffected factors are shown in gray. The expression of *Xbp1* (XBP-1), as well as numerous XBP-1-induced genes (shown in the orange box), are reduced by morphine, as are several endoplasmic reticulum (ER) chaperone proteins involved in ER quality control (ERQC). These chaperones assist in the proper folding and export of proteins or target misfolded proteins to the proteasome by a process known as ER-associated degradation (ERAD). The downregulation of these factors might lead to the increased accumulation and/or export of misfolded proteins, including myelin constituents.

OL-specific expression of *Myc*, as well as *Sox2* and *Sox10*, key drivers of OPC identity. *Sox10* expression is downregulated in the brains of rats following heroin self-administration (Martin et al., 2018). Our single-cell analyses revealed that a significant number of GR-regulated genes are induced by morphine in OLs. Morphine rapidly increases serum levels of corticosterone (Simon et al., 1975), which in turn induces expression of *Sgk1* (Miyata et al., 2011). GR signaling is critical for morphine-dependent dopamine release and locomotor activation in mice (Marinelli et al., 1998), but the contributions of OLs to these phenotypes have not been examined. Presumably, the morphine-dependent induction of *Sgk1* and a subset of the other genes we identified occurs via GR-dependent transcriptional activation. The robust induction of *Sgk1* we observed is particularly intriguing, because this gene facilitates morphological changes in OLs that are associated with depressive-like behaviors (Miyata et al., 2015). Alterations in OL morphology have also been observed in morphine-treated mice (Hauser et al., 2009). Thus, the morphine-dependent induction of *Sgk1* specifically in OLs constitutes a putative molecular mechanism underlying depressive-like behaviors in opioid-dependent individuals. It was previously suggested that morphine- and GR-dependent gene expression changes (including *Sgk1* induction) are largely confined to astrocytes (Slezak et al., 2013). However, our single-cell analyses indicate that many GR-dependent genes are induced uniquely in either OLs (i.e., *Sgk1* and *Sgk3*) or astrocytes (i.e., *Tsc22d3* and *Gjb6*), whereas others are induced in both of these cell types (i.e., *Fkbp5* and *Nfkbia*). Cell-type-specific expression patterns of opioid receptor subtypes and GR may explain the shared and unique gene expression changes we observed in neurons, astrocytes, and OLs. Unfortunately, because opioid receptor genes are relatively lowly expressed, they were only sparsely detected in our single-cell data, obfuscating our attempts to correlate patterns of opioid receptor expression with the observed transcriptional response to morphine. Regarding the mechanism of the response by OLs, our FISH data suggest that opioid receptor activation is critical, but the relative contributions of OL-, neuron-, and/or astrocyte-derived opioid receptors remain unknown. Our *in vitro* data indicate that a non-cell-autonomous mechanism is likely, but they do not exclude the possibility of OL-specific, GR-mediated effects. We also cannot rule out the putative contributions of other indirect mechanisms, including neuronal activity-dependent responses and paracrine regulation by neurons, astrocytes, and/or microglia.

Our pathway analysis revealed highly significant morphine-dependent downregulation of genes encoding heat shock proteins, ER chaperones, and other factors critically involved in the UPR and ER quality control (ERQC). The expression of heat shock proteins, including Hsp70 (*Hspa1a*) and Hsc70 (*Hspa8*), has previously been shown to be modulated by morphine treatment of rats (Ammon-Treiber et al., 2004; Salas et al., 2011). Proper regulation of the UPR is essential for efficient myelination, as evidenced by the apparent dysregulation of UPR in multiple myelin disorders, including Charcot-Marie-Tooth disease, vanishing white matter disease, and multiple sclerosis (Lin and Popko, 2009; Volpi et al., 2017). Under normal conditions, GRP78/BiP (encoded by *Hspa5*) is thought to initiate the UPR by sensing misfolded proteins in the ER (Volpi et al., 2017), and its conditional ablation in OLs or Schwann cells results in cell death and severe hypomyelination (Hussien et al., 2015). Coincidentally, *Hspa5* is also the most significantly morphine-repressed gene that we detected in OLs. The reduced expression of downstream response genes, including the anti-survival gene CHOP (*Ddit3*) and several ER chaperone proteins, suggests that morphine potently suppresses the canonical UPR, which normally entails attenuation of global protein synthesis, degradation of misfolded proteins, and under severe ER stress, autophagy or apoptosis. Previous studies suggested that perinatal exposure to other opioid drugs, specifically buprenorphine and methadone, appears to promote myelination (Eschenroeder et al., 2012; Sanchez et al., 2008; Vestal-Laborde et al., 2014). Perhaps in the context of chronic opioid exposure, persistent upregulation of myelin synthesis and concomitant downregulation of ERQC leads to increased accumulation and/or export of misfolded myelin constituents and therefore altered myelin composition. The integrity and composition of myelin have not been investigated in models of long-term morphine exposure.

In summary, we used scRNA-seq to enable the elucidation of cell-type-specific responses to morphine in the NAc of mice. We identified a dramatic transcriptional response by OLs and shed

light on the underlying molecular mechanisms of this response, specifically implicating GR signaling and the UPR as potential links between gene expression changes we observed and opioid-mediated myelin pathology. Our single-cell and bulk RNA-seq datasets should serve as valuable resources for research aiming to assess transcriptional responses to opioids or other drugs of abuse. Future studies are necessary to investigate the mechanisms, functional consequences, and physiological significance of oligodendrocyte-opioid interactions.

STAR★METHODS

Detailed methods are provided in the online version of this paper and include the following:

- KEY RESOURCES TABLE
- CONTACT FOR REAGENT AND RESOURCE SHARING
- EXPERIMENTAL MODEL AND SUBJECT DETAILS
  - Mice
- METHOD DETAILS
  - Dissection and tissue dissociation
  - Drop-seq library generation and QC
  - Unsupervised clustering and dimensionality reduction
  - scRNA-seq analysis
  - Morphine-activated score
  - *In situ* hybridization
  - Imaging and image analysis
  - *In vitro* OL culture
  - Cnp-Cre/Ribotag RNA isolation
  - Quantitative real-time PCR
  - Immunostaining and FACS of OLs
  - RNA purification, library prep, and sequencing
  - RNaseq alignment and DE analysis
  - Pathway analysis of RNaseq data
- QUANTIFICATION AND STATISTICAL ANALYSIS
  - Single-cell analysis
  - FISH
  - qRT-PCR
- DATA AND SOFTWARE AVAILABILITY

SUPPLEMENTAL INFORMATION

Supplemental Information includes nine figures and five tables and can be found with this article online at https://doi.org/10.1016/j.celrep.2018.08.080.

ACKNOWLEDGMENTS

This work was supported by NIH grants CA009547-33 (to D.A.), AGO13730 and NS099314 (to J.M.), and 5U01MH109133, RF1MH117070, and R01GM129126 (to R.D.M.) and the Intellectual and Developmental Disabilities Research Center at Washington University (U54 HD087011). We thank the Alvin J. Siteman Cancer Center at Washington University School of Medicine and Barnes-Jewish Hospital in St. Louis for the use of the Siteman Flow Cytometry core. The Siteman Cancer Center is supported in part by an NCI Cancer Center support grant (P30 CA091842). We thank Peter Wang and Gwendalyn Randolph for sharing the CD45-PacBlue antibody.

AUTHOR CONTRIBUTIONS

Conceptualization, D.A., R.D.M., and J.M.; Methodology, D.A.; Software, D.A., S.S., and A.K.Y.Y.; Validation, D.A.; Formal Analysis, D.A., S.S., A.K.Y.Y., and R.B.; Investigation, D.A.; Resources, R.D.M. and J.M.; Data Curation, D.A. and S.S.; Writing – Original Draft, D.A.; Writing – Review & Editing, D.A., R.D.M., and J.M.; Visualization, D.A. and R.B.; Supervision, R.D.M. and J.M.; Funding Acquisition, D.A., R.D.M., and J.M.

DECLARATION OF INTERESTS

The authors declare no competing interests.

Received: May 10, 2018
Revised: July 3, 2018
Accepted: August 24, 2018
Published: September 25, 2018

REFERENCES

Albertson, D.N., Schmidt, C.J., Kapatos, G., and Bannon, M.J. (2006). Distinctive profiles of gene expression in the human nucleus accumbens associated with cocaine and heroin abuse. Neuropsychopharmacology *31*, 2304–2312.

Ammon-Treiber, S., Grecksch, G., Stumm, R., Riechert, U., Tischmeyer, H., Reichenauer, A., and Höllt, V. (2004). Rapid, transient, and dose-dependent expression of hsp70 messenger RNA in the rat brain after morphine treatment. Cell Stress Chaperones *9*, 182–197.

Bach, A.G., Jordan, B., Wegener, N.A., Rusner, C., Kornhuber, M., Abbas, J., and Surov, A. (2012). Heroin spongiform leukoencephalopathy (HSLE). Clin. Neuroradiol. *22*, 345–349.

Bauer, I.E., Soares, J.C., and Nielsen, D.A. (2015). The role of opioidergic genes in the treatment outcome of drug addiction pharmacotherapy: a systematic review. Am. J. Addict. *24*, 15–23.

Bora, E., Yücel, M., Fornito, A., Pantelis, C., Harrison, B.J., Cocchi, L., Pell, G., and Lubman, D.I. (2012). White matter microstructure in opiate addiction. Addict. Biol. *17*, 141–148.

Butler, A., Hoffman, P., Smibert, P., Papalexi, E., and Satija, R. (2018). Integrating single-cell transcriptomic data across different conditions, technologies, and species. Nat. Biotechnol. *36*, 411–420.

Campbell, J.N., Macosko, E.Z., Fenselau, H., Pers, T.H., Lyubetskaya, A., Tenen, D., Goldman, M., Verstegen, A.M., Resch, J.M., McCarroll, S.A., et al. (2017). A molecular census of arcuate hypothalamus and median eminence cell types. Nat. Neurosci. *20*, 484–496.

Cao, J., Packer, J.S., Ramani, V., Cusanovich, D.A., Huynh, C., Daza, R., Qiu, X., Lee, C., Furlan, S.N., Steemers, F.J., et al. (2017). Comprehensive single-cell transcriptional profiling of a multicellular organism. Science *357*, 661–667.

Dal Molin, A., Baruzzo, G., and Di Camillo, B. (2017). Single-cell RNA-sequencing: assessment of differential expression analysis methods. Front. Genet. *8*, 62.

Dart, R.C., Surratt, H.L., Cicero, T.J., Parrino, M.W., Severtson, S.G., Bucher-Bartelson, B., and Green, J.L. (2015). Trends in opioid analgesic abuse and mortality in the United States. N. Engl. J. Med. *372*, 241–248.

Dincman, T.A., Beare, J.E., Ohri, S.S., and Whittemore, S.R. (2012). Isolation of cortical mouse oligodendrocyte precursor cells. J. Neurosci. Methods *209*, 219–226.

Du, C., Duan, Y., Wei, W., Cai, Y., Chai, H., Lv, J., Du, X., Zhu, J., and Xie, X. (2016). Kappa opioid receptor activation alleviates experimental autoimmune encephalomyelitis and promotes oligodendrocyte-mediated remyelination. Nat. Commun. *7*, 11120.

Enoksson, T., Bertran-Gonzalez, J., and Christie, M.J. (2012). Nucleus accumbens D2- and D1-receptor expressing medium spiny neurons are selectively activated by morphine withdrawal and acute morphine, respectively. Neuropharmacology *62*, 2463–2471.

Eschenroeder, A.C., Vestal-Laborde, A.A., Sanchez, E.S., Robinson, S.E., and Sato-Bigbee, C. (2012). Oligodendrocyte responses to buprenorphine uncover novel and opposing roles of μ-opioid- and nociceptin/orphanin FQ receptors in cell development: implications for drug addiction treatment during pregnancy. Glia *60*, 125–136.

Gokce, O., Stanley, G.M., Treutlein, B., Neff, N.F., Camp, J.G., Malenka, R.C., Rothwell, P.E., Fuccillo, M.V., Südhof, T.C., and Quake, S.R. (2016). Cellular taxonomy of the mouse striatum as revealed by single-cell RNA-seq. Cell Rep. *16*, 1126–1137.

Hauser, K.F., Stiene-Martin, A., Mattson, M.P., Elde, R.P., Ryan, S.E., and Godleske, C.C. (1996). mu-Opioid receptor-induced Ca2+ mobilization and astroglial development: morphine inhibits DNA synthesis and stimulates cellular hypertrophy through a Ca(2+)-dependent mechanism. Brain Res. *720*, 191–203.

Hauser, K.F., Hahn, Y.K., Adjan, V.V., Zou, S., Buch, S.K., Nath, A., Bruce-Keller, A.J., and Knapp, P.E. (2009). HIV-1 Tat and morphine have interactive effects on oligodendrocyte survival and morphology. Glia *57*, 194–206.

Hodes, G.E., Pfau, M.L., Purushothaman, I., Ahn, H.F., Golden, S.A., Christoffel, D.J., Magida, J., Brancato, A., Takahashi, A., Flanigan, M.E., et al. (2015). Sex differences in nucleus accumbens transcriptome profiles associated with susceptibility versus resilience to subchronic variable stress. J. Neurosci. *35*, 16362–16376.

Hussien, Y., Podojil, J.R., Robinson, A.P., Lee, A.S., Miller, S.D., and Popko, B. (2015). ER chaperone BiP/GRP78 is required for myelinating cell survival and provides protection during experimental autoimmune encephalomyelitis. J. Neurosci. *35*, 15921–15933.

Islam, S., Zeisel, A., Joost, S., La Manno, G., Zajac, P., Kasper, M., Lönnerberg, P., and Linnarsson, S. (2014). Quantitative single-cell RNA-seq with unique molecular identifiers. Nat. Methods *11*, 163–166.

Kharchenko, P.V., Silberstein, L., and Scadden, D.T. (2014). Bayesian approach to single-cell differential expression analysis. Nat. Methods *11*, 740–742.

Klein, A.M., Mazutis, L., Akartuna, I., Tallapragada, N., Veres, A., Li, V., Peshkin, L., Weitz, D.A., and Kirschner, M.W. (2015). Droplet barcoding for single-cell transcriptomics applied to embryonic stem cells. Cell *161*, 1187–1201.

Knapp, P.E., and Hauser, K.F. (1996). mu-Opioid receptor activation enhances DNA synthesis in immature oligodendrocytes. Brain Res. *743*, 341–345.

Knapp, P.E., Maderspach, K., and Hauser, K.F. (1998). Endogenous opioid system in developing normal and jimpy oligodendrocytes: mu and kappa opioid receptors mediate differential mitogenic and growth responses. Glia *22*, 189–201.

Korostynski, M., Piechota, M., Kaminska, D., Solecki, W., and Przewlocki, R. (2007). Morphine effects on striatal transcriptome in mice. Genome Biol. *8*, R128.

Li, W., Zhu, J., Li, Q., Ye, J., Chen, J., Liu, J., Li, Z., Li, Y., Yan, X., Wang, Y., and Wang, W. (2016). Brain white matter integrity in heroin addicts during methadone maintenance treatment is related to relapse propensity. Brain Behav. *6*, e00436.

Lin, W., and Popko, B. (2009). Endoplasmic reticulum stress in disorders of myelinating cells. Nat. Neurosci. *12*, 379–385.

Liu, H., Li, L., Hao, Y., Cao, D., Xu, L., Rohrbaugh, R., Xue, Z., Hao, W., Shan, B., and Liu, Z. (2008). Disrupted white matter integrity in heroin dependence: a controlled study utilizing diffusion tensor imaging. Am. J. Drug Alcohol Abuse *34*, 562–575.

Lobo, M.K., Karsten, S.L., Gray, M., Geschwind, D.H., and Yang, X.W. (2006). FACS-array profiling of striatal projection neuron subtypes in juvenile and adult mouse brains. Nat. Neurosci. *9*, 443–452.

Lun, A.T., Bach, K., and Marioni, J.C. (2016). Pooling across cells to normalize single-cell RNA sequencing data with many zero counts. Genome Biol. *17*, 75.

Lüscher, C., and Malenka, R.C. (2011). Drug-evoked synaptic plasticity in addiction: from molecular changes to circuit remodeling. Neuron *69*, 650–663.

Macosko, E.Z., Basu, A., Satija, R., Nemesh, J., Shekhar, K., Goldman, M., Tirosh, I., Bialas, A.R., Kamitaki, N., Martersteck, E.M., et al. (2015). Highly parallel genome-wide expression profiling of individual cells using nanoliter droplets. Cell *161*, 1202–1214.

Marinelli, M., Aouizerate, B., Barrot, M., Le Moal, M., and Piazza, P.V. (1998). Dopamine-dependent responses to morphine depend on glucocorticoid receptors. Proc. Natl. Acad. Sci. USA *95*, 7742–7747.

Marques, S., Zeisel, A., Codeluppi, S., van Bruggen, D., Mendanha Falcão, A., Xiao, L., Li, H., Häring, M., Hochgerner, H., Romanov, R.A., et al. (2016). Oligodendrocyte heterogeneity in the mouse juvenile and adult central nervous system. Science *352*, 1326–1329.

Martin, J.A., Caccamise, A., Werner, C.T., Viswanathan, R., Polanco, J.J., Stewart, A.F., Thomas, S.A., Sim, F.J., and Dietz, D.M. (2018). A novel role for oligodendrocyte precursor cells (OPCs) and Sox10 in mediating cellular and behavioral responses to heroin. Neuropsychopharmacology *43*, 1385–1394.

McCarthy, D.J., Campbell, K.R., Lun, A.T., and Wills, Q.F. (2017). Scater: pre-processing, quality control, normalization and visualization of single-cell RNA-seq data in R. Bioinformatics *33*, 1179–1186.

Mei, F., Mayoral, S.R., Nobuta, H., Wang, F., Desponts, C., Lorrain, D.S., Xiao, L., Green, A.J., Rowitch, D., Whistler, J., and Chan, J.R. (2016). Identification of the kappa-opioid receptor as a therapeutic target for oligodendrocyte remyelination. J. Neurosci. *36*, 7925–7935.

Miyata, S., Koyama, Y., Takemoto, K., Yoshikawa, K., Ishikawa, T., Taniguchi, M., Inoue, K., Aoki, M., Hori, O., Katayama, T., and Tohyama, M. (2011). Plasma corticosterone activates SGK1 and induces morphological changes in oligodendrocytes in corpus callosum. PLoS ONE *6*, e19859.

Miyata, S., Hattori, T., Shimizu, S., Ito, A., and Tohyama, M. (2015). Disturbance of oligodendrocyte function plays a key role in the pathogenesis of schizophrenia and major depressive disorder. BioMed Res. Int. *2015*, 492367.

Palazuelos, J., Klingener, M., and Aguirre, A. (2014). TGFβ signaling regulates the timing of CNS myelination by modulating oligodendrocyte progenitor cell cycle exit through SMAD3/4/FoxO1/Sp1. J. Neurosci. *34*, 7917–7930.

Piechota, M., Korostynski, M., Solecki, W., Gieryk, A., Slezak, M., Bilecki, W., Ziolkowska, B., Kostrzewa, E., Cymerman, I., Swiech, L., et al. (2010). The dissection of transcriptional modules regulated by various drugs of abuse in the mouse striatum. Genome Biol. *11*, R48.

Qiu, X., Mao, Q., Tang, Y., Wang, L., Chawla, R., Pliner, H.A., and Trapnell, C. (2017). Reversed graph embedding resolves complex single-cell trajectories. Nat. Methods *14*, 979–982.

Robinson, A.P., Rodgers, J.M., Goings, G.E., and Miller, S.D. (2014). Characterization of oligodendroglial populations in mouse demyelinating disease using flow cytometry: clues for MS pathogenesis. PLoS ONE *9*, e107649.

Salas, E., Bocos, C., Del Castillo, C., Pérez-García, C., Morales, L., and Alguacil, L.F. (2011). Gene expression analysis of heat shock proteins in the nucleus accumbens of rats with different morphine seeking behaviours. Behav. Brain Res. *225*, 71–76.

Sanchez, E.S., Bigbee, J.W., Fobbs, W., Robinson, S.E., and Sato-Bigbee, C. (2008). Opioid addiction and pregnancy: perinatal exposure to buprenorphine affects myelination in the developing brain. Glia *56*, 1017–1027.

Sanz, E., Yang, L., Su, T., Morris, D.R., McKnight, G.S., and Amieux, P.S. (2009). Cell-type-specific isolation of ribosome-associated mRNA from complex tissues. Proc. Natl. Acad. Sci. USA *106*, 13939–13944.

Satija, R., Farrell, J.A., Gennert, D., Schier, A.F., and Regev, A. (2015). Spatial reconstruction of single-cell gene expression data. Nat. Biotechnol. *33*, 495–502.

Saxena, A., Wagatsuma, A., Noro, Y., Kuji, T., Asaka-Oba, A., Watahiki, A., Gurnot, C., Fagiolini, M., Hensch, T.K., and Carninci, P. (2012). Trehalose-enhanced isolation of neuronal sub-types from adult mouse brain. Biotechniques *52*, 381–385.

Schindelin, J., Arganda-Carreras, I., Frise, E., Kaynig, V., Longair, M., Pietzsch, T., Preibisch, S., Rueden, C., Saalfeld, S., Schmid, B., et al. (2012). Fiji: an open-source platform for biological-image analysis. Nat. Methods *9*, 676–682.

Simon, M., George, R., and Garcia, J. (1975). Acute morphine effects on regional brain amines, growth hormone and corticosterone. Eur. J. Pharmacol. *34*, 21–26.

Skupio, U., Sikora, M., Korostynski, M., Wawrzczak-Bargiela, A., Piechota, M., Ficek, J., and Przewlocki, R. (2017). Behavioral and transcriptional patterns of protracted opioid self-administration in mice. Addict. Biol. *22*, 1802–1816.

Slezak, M., Korostynski, M., Gieryk, A., Golda, S., Dzbek, J., Piechota, M., Wlazlo, E., Bilecki, W., and Przewlocki, R. (2013). Astrocytes are a neural target of morphine action via glucocorticoid receptor-dependent signaling. Glia *61*, 623–635.

Stiene-Martin, A., and Hauser, K.F. (1991). Glial growth is regulated by agonists selective for multiple opioid receptor types *in vitro*. J. Neurosci. Res. *29*, 538–548.

Stiene-Martin, A., Knapp, P.E., Martin, K., Gurwell, J.A., Ryan, S., Thornton, S.R., Smith, F.L., and Hauser, K.F. (2001). Opioid system diversity in developing neurons, astroglia, and oligodendroglia in the subventricular zone and striatum: impact on gliogenesis *in vivo*. Glia *36*, 78–88.

Treutlein, B., Lee, Q.Y., Camp, J.G., Mall, M., Koh, W., Shariati, S.A., Sim, S., Neff, N.F., Skotheim, J.M., Wernig, M., and Quake, S.R. (2016). Dissecting direct reprogramming from fibroblast to neuron using single-cell RNA-seq. Nature *534*, 391–395.

Upadhyay, J., Maleki, N., Potter, J., Elman, I., Rudrauf, D., Knudsen, J., Wallin, D., Pendse, G., McDonald, L., Griffin, M., et al. (2010). Alterations in brain structure and functional connectivity in prescription opioid-dependent patients. Brain *133*, 2098–2114.

van der Maaten, L.H.G. (2008). Visualizing data using t-SNE. J. Mach. Learn. Res. *9*, 2579–2605.

Vestal-Laborde, A.A., Eschenroeder, A.C., Bigbee, J.W., Robinson, S.E., and Sato-Bigbee, C. (2014). The opioid system and brain development: effects of methadone on the oligodendrocyte lineage and the early stages of myelination. Dev. Neurosci. *36*, 409–421.

Volkow, N.D., and Morales, M. (2015). The brain on drugs: from reward to addiction. Cell *162*, 712–725.

Volpi, V.G., Touvier, T., and D'Antonio, M. (2017). Endoplasmic reticulum protein quality control failure in myelin disorders. Front. Mol. Neurosci. *9*, 162.

Wang, Y., Li, W., Li, Q., Yang, W., Zhu, J., and Wang, W. (2011). White matter impairment in heroin addicts undergoing methadone maintenance treatment and prolonged abstinence: a preliminary DTI study. Neurosci. Lett. *494*, 49–53.

Zezula, J., Casaccia-Bonnefil, P., Ezhevsky, S.A., Osterhout, D.J., Levine, J.M., Dowdy, S.F., Chao, M.V., and Koff, A. (2001). p21cip1 is required for the differentiation of oligodendrocytes independently of cell cycle withdrawal. EMBO Rep. *2*, 27–34.

Zhang, Y., Chen, K., Sloan, S.A., Bennett, M.L., Scholze, A.R., O'Keeffe, S., Phatnani, H.P., Guarnieri, P., Caneda, C., Ruderisch, N., et al. (2014). An RNA-sequencing transcriptome and splicing database of glia, neurons, and vascular cells of the cerebral cortex. J. Neurosci. *34*, 11929–11947.

Zheng, G.X., Terry, J.M., Belgrader, P., Ryvkin, P., Bent, Z.W., Wilson, R., Ziraldo, S.B., Wheeler, T.D., McDermott, G.P., Zhu, J., et al. (2017). Massively parallel digital transcriptional profiling of single cells. Nat. Commun. *8*, 14049.

Zhu, L., Zhu, J., Liu, Y., Chen, Y., Li, Y., Chen, S., Li, T., Dang, Y., and Chen, T. (2015). Chronic methamphetamine regulates the expression of MicroRNAs and putative target genes in the nucleus accumbens of mice. J. Neurosci. Res. *93*, 1600–1610.

STAR★METHODS

KEY RESOURCES TABLE

REAGENT or RESOURCE	SOURCE	IDENTIFIER
Antibodies		
Anti-Mog	Millipore	Cat# MAB5680; RRID:AB_1587278
Anti-GalC-FITC	Millipore	Cat# FCMAB312F; RRID:AB_10806360
Anti-PDGFRα-PE	BD Biosciences	Cat # 562776; RRID:AB_657615
Anti-CD45-Pacific Blue	BioLegend	Cat# 103126; RRID:AB_493535
CD140a (PDGFRα) MicroBead Kit	Miltenyi Biotech	130-101-547
Chemicals, Peptides, and Recombinant Proteins		
Trehalose	Sigma-Aldrich	T5251; CAS: 6138-23-4
Neural Tissue Dissociation Kit	Miltenyi Biotech	103-092-628
Critical Commercial Assays		
Lightning Link Rapid Cy5	Novus Biosciences	342-0010
ViewRNA ISH Cell Assay	Thermo Fisher	QVC-0001
MiniMACS Separator	Miltenyi Biotech	130-042-102
Deposited Data		
Raw and analyzed data	This paper	GSE118918
Experimental Models: Organisms/Strains		
C57BL/6 mice (male; 6-12 weeks)	Jackson Laboratory	N/A
Cnp-Cre mice	N/A	N/A
Rpl22-HA (Ribotag) mice	Sanz et al., 2009	N/A
Cnp-Cre x Ribotag mice	This paper	N/A
Oligonucleotides		
*See Table S4 for list of primers used for qRT-PCR	N/A	N/A
Software and Algorithms		
Seurat	Satija et al., 2015	http://satijalab.org/seurat/
Monocle	Qiu et al., 2017	http://cole-trapnell-lab.github.io/monocle-release/
SCDE	Kharchenko et al., 2014	http://hms-dbmi.github.io/scde/

CONTACT FOR REAGENT AND RESOURCE SHARING

Further information and requests for resources and reagents should be directed to and will be fulfilled by the Lead Contact, Robi Mitra (rmitra@wustl.edu).

EXPERIMENTAL MODEL AND SUBJECT DETAILS

Mice

All animal care and experimental procedures were approved in advance by the National Institute of Health and Washington University School of Medicine Institutional Animal Care and Use Committee (Protocol #20170030). Male C57BL/6 mice (6-12 weeks old) were used for all experiments, and all animals were socially housed on a 12 h light dark cycle with water and food *ad libitum*. Mice were injected with saline or morphine sulfate (20 mg/kg) intraperitoneally, and/or naltrexone hydrochloride (2 mg/kg) subcutaneously. Cnp-Cre mice were crossed with Rpl22-HA ("RiboTag") (Sanz et al., 2009) mice (both in the C57BL/6 background) to generate Cnp-Cre x RiboTag mice, facilitating the immunoprecipitation of oligodendrocyte-enriched mRNAs for qRT-PCR analysis.

METHOD DETAILS

Dissection and tissue dissociation

Four h after saline (mock) or morphine injection, mice were anesthetized by isoflurane and euthanized by decapitation. Brains were rapidly extracted, cooled in ice-cold Hibernate A (-Ca) media for 5 min, then placed ventral surface up onto a chilled Petri dish on ice.

The rostral and caudal boundaries of the NAc were visually approximated and a ~1 mm-thick coronal section was obtained using a chilled razor blade. The NAc was microdissected at its dorsolateral borders and pooled by experimental condition (two mice per replicate). Pooled tissue samples were digested in papain/DNase I solution for 1 h at 37°C, according to a previously published protocol (Saxena et al., 2012). The final volume was 1 mL per mouse NAc. Digestion was stopped by dilution with EBSS #2 (Saxena et al., 2012), which contains ovomucoid protease inhibitor. Tissue was centrifuged at 300*g* for 5 min, resuspended in EBSS #2, then gently triturated with a P200 pipette. The resulting cell suspension was divided between two microfuge tubes and diluted with Drop-seq buffer to a volume of 1 mL per tube (per 2 pooled samples). Drop-seq buffer consisted of 5% (wt/vol) trehalose, Hank's buffered salt solution (HBSS; magnesium- and calcium-free), 2.13 mM $MgCl_2$, 2 mM $MgSO_4$, 1.26 mM $CaCl_2$, 1 mM glucose and 0.02% bovine serum albumin. Cells were washed twice by centrifugation at 300*g* for 5 min, followed by resuspension in 1 mL Drop-seq buffer. Cells were then passed through a 40-μm mesh filter, diluted to 210 cells/μL using cell concentration estimates from a hemocytometer, and kept on ice until use (< 30 min).

Drop-seq library generation and QC

Drop-seq was performed as previously described (Campbell et al., 2017). Mouse NAc suspensions were processed through Drop-Seq in eight separate groups over four separate batches (one batch per day). Libraries were sequenced on the Illumina HiSeq3000 or HiSeq2500. Read 1 was 25 bp (bases 1–12 cell barcode, bases 13–20 UMI – unique molecular identifier), read 2 (paired end) was 75 bp, and the index primer was 7 bp. Raw sequence data were first filtered to remove all read pairs with a barcode base quality of less than 10. The second read (75 bp) was then trimmed at the 5′ end to remove any TSO adaptor sequence and at the 3′ end to remove poly(A) tails of length 6 or greater, then aligned to the mouse (mm10) genome using STAR v2.4.2a with default settings. Uniquely mapped reads were grouped by cell barcode. A list of UMIs in each gene, within each cell, was assembled, and UMIs within ED = 1 were merged together. The total number of unique UMI sequences was counted, and this number was reported as the number of transcripts of that gene for a given cell.

All cell barcodes in which 500 or more genes *and* 1000 or more transcripts (UMIs) were detected were used in downstream analysis. Raw digital expression matrices were generated separately, then the replicates from each experimental group were merged together into a single matrix. Cells with high expression levels of one or more marker gene(s) of more than one cell type (i.e., neuron, oligodendrocyte, astrocyte, endothelial cell, etc.), representing likely cell doublets/multiplets, were removed (~4% of all STAMPS), resulting in a 12,105-cell barcode dataset for mock treatment and a 11,171-cell barcode dataset for morphine treatment. Gene expression was normalized in Scater (McCarthy et al., 2017) using the method described by Lun et al. (Lun et al., 2016), and genes with expression in ≥ 50 cells were retained for clustering. Before clustering, we removed unwanted variation due to number of UMIs, ratio of reads mapping to mitochondrial genes, and batch effects using Seurat software (Satija et al., 2015).

Unsupervised clustering and dimensionality reduction

We used Seurat to perform clustering (Butler et al., 2018; Satija et al., 2015). We identified genes that were most variable across the entire dataset, controlling for the known relationship between mean expression and variance. We calculated the mean and dispersion (variance/mean) for each gene across all cells, then identified outlier genes. To distinguish principal components (PCs) for further analysis, we used the PCElbowPlot() function, and found that PCs beyond 15 accounted for negligible variance. We identified molecularly distinct clusters using the FindClusters() function with the Louvain algorithm with multilevel refinement, using a high resolution (2.0) to detect weakly distinguishable clusters. We then built a classification hierarchy, merged clusters with higher than 0.05 Out-of-bag error (OOBE) from a random forest classifier, and performed *t*-distributed stochastic neighbor embedding (t-SNE) (van der Maaten, 2008) in Seurat with default settings. This allowed us to assign cells into a total of 18 cell type clusters each for mock and morphine. To further resolve cell subtypes, cells corresponding to neuronal, oligodendrocyte, or other clusters were combined, then iteratively clustered as above using CCA (Butler et al., 2018). Altogether, we identified 29 molecularly distinct cell types, all of which were shared between mock- and morphine-treated mice.

scRNA-seq analysis

To analyze differential gene expression between morphine and mock datasets, we performed pairwise differential expression analysis on specific cell subpopulations using the SCDE package, which fits individual error models to account for stochastic detection of lowly expressed genes (Kharchenko et al., 2014). We included all Seurat-generated clusters containing > 10 cells from each of 8 biological replicates (Mock1-4, Morphine1-4), and that had relatively uniform distribution across all replicates. Only 3 neuronal subtypes (cholinergic interneurons, D1 MSN_*Cxcl14*$^+$, and D1 MSN_*Pcdh8*$^+$) did not meet these criteria. We used default settings with the exception that we varied the min.detected parameter of the clean.counts function to filter out genes detected in less than 2% of cells. We included the results of every cluster for all gene with p value < 0.5 in Table S2.

Morphine-activated score

Score was generated for each cell of the OL lineage using quadratic programming, as previously described (Treutlein et al., 2016) with the following modifications. Briefly, we log-transformed transcript counts from FACS-RNaseq data of OLs (average of 3 mock or 3 morphine samples). We used this as mock and morphine reference profiles after filtering out genes not appreciably detected by Drop-seq of OLs (genes detected in < 5% of cells). The R package QuadProg was used for quadratic programming to assign a

mock score and a morphine score to each single cell from the OL lineage. The values shown in Figure S4 were calculated by dividing the morphine score by the sum of the mock score and the morphine score to obtain a scaled morphine-activated score (from 0 to 1).

In situ hybridization

Morphine and mock treatments were performed as described above, except that mock treatment was preceded by a subcutaneous (s.c.) saline injection (Ctrl/Ctrl), and morphine treatment was preceded by injection with s.c. saline (Ctrl/Morphine) or naltrexone (NTX/Morphine). After 4 h, brains were harvested and immediately flash-frozen in OCT (optimal cutting temperature compound) in liquid nitrogen. We stored frozen tissue blocks at −80°C prior to sectioning. Twelve-micron thick coronal sections were cut at −20°C and adhered to positively charged Leica slides (one of each of the three treatment conditions per slide), then stored at −80°C. Frozen tissue sections were washed briefly with 1X PBS and fixed in 3.7% para-formaldehyde for 1 h. Following fixation, slides were washed twice with 1X PBS and then submerged in 70% ethanol overnight at 4°C for permeabilization. RNA FISH was performed according to the Affymetrix ViewRNA protocol.

Imaging and image analysis

We imaged FISH AND IHC slides on a Zeiss LSM 880 II confocal microscope at the Washington University Center for Cellular Imaging (WUCCI). Image files were processed and analyzed in Fiji/ImageJ (Schindelin et al., 2012) software. RGB channels corresponding to the two Affymetrix probes and DAPI were split. RNA particles in each channel were then identified in a semi-automated manner by selecting an intensity threshold above which a spot is considered an RNA particle. Numbers of puncta per cell were quantified from the left and right anterior commissures, the corpus callosum, and the NAc (n = 3 mice per treatment).

In vitro OL culture

We isolated, expanded, and differentiated OPCs into OLs as previously described (Dincman et al., 2012). Briefly, we dissociated cells from postnatal day 6 (P6) mouse cortices using the papain-based Neural Tissue Dissociation Kit (Miltenyi) and mechanical trituration, then enriched for OPCs using magnetic cell sorting (MACS) with anti-PDGFRα-conjugated microbeads and a miniMACS separator. OPCs were expanded for 3 days, passaged to new plates, then differentiated for 6 days (or maintained in proliferation media and harvested as OPCs). On the sixth day (D6), cells were mock-treated with media, or treated with a low (0.5 μg/ml) or high (5 μg/ml) dose of morphine sulfate, then harvested for qRT-PCR at 3 h post-treatment. Values shown in Figure S6 are means from three biological replicates.

Cnp-Cre/Ribotag RNA isolation

Mock/morphine treatment and dissection was performed as described above, except that the entire striatum, corpus callosum, or 40 mg of cortex were harvested and transferred to microcentrifuge tubes containing 500 μL polysome lysis buffer. Lysis and immunoprecipitation were performed as previously described (Sanz et al., 2009). Lysates were applied to Machery Nagel Nucleospin RNA columns and RNA was purified per the manufacturer's protocol.

Quantitative real-time PCR

RNA isolated from Cnp-Cre x Ribotag mice or FACS-isolated OLs (see below) was reverse transcribed using qScript cDNA Supermix from QuantaBio according to the manufacturer's protocol. cDNA was mixed with Fast SYBR Green master mix from ThermoFisher and primers to the indicated gene (see Table S4 for primer sequences) in a 96-well plate and quantified using the Quant Studio 3 from Applied Biosciences (in technical triplicates). Differences in relative gene expression were calculated using the delta delta cT method after normalization to beta-actin.

Immunostaining and FACS of OLs

WT mice were injected with saline (mock) or morphine as described above. Four h later, mice were euthanized and entire brains were removed, minced with a razor blade, and dissociated with papain solution (400 units of papain in 8 mL total volume). After 50 min dissociation, suspensions were diluted with EBSS #2 (Saxena et al., 2012), serially passed through 100 μm and 40 μm filters, and centrifuged at 300*g* for 5 min. The pellet was resuspended in 35% Percoll solution prepared in EBSS containing 0.1% BSA and 5% trehalose, then centrifuged at 800*g* for 20 min at 18°C. The supernatant containing myelin and cell debris was carefully removed and the pellet was resuspended in flow cytometry buffer (1% normal mouse serum, 1% normal rat serum, 5% trehalose, 0.1% BSA, 1 mM EDTA in DPBS). Cells were counted using a hemocytometer and ~3e6 cells were transferred to a fresh tube, pelleted by brief centrifugation at 300*g*, and resuspended in 200 μL flow cytometry buffer containing the following fluorophore-conjugated antibodies (or isotype controls): GalC-FITC (4 μg; Millipore), PDGFRa-PE (2 μg; BD Biosciences), Mog-Cy5 (4 μg; Millipore; conjugated with Lightning Link kit from Novus Bio), and CD45-PacBlue (2 μg; BioLegend). Tubes were incubated at 4°C with gentle rotation for 30 min, protected from light. Cells were washed twice with and resuspended in flow cytometry buffer (500 μL) and stored on ice protected from light until sorting (< 30 min). Samples were sorted into flow cytometry buffer using the Sony SY3200 "Synergy" with 100 μm nozzle size at the Siteman Cancer Center Flow Cytometry Core.

RNA purification, library prep, and sequencing

Immediately following FACS, cells (~100K per sample) were centrifuged at 300*g* for 5 min at 4°C, and the supernatant was carefully removed. The pellet was resuspended in 300 μL Trizol reagent and RNA was purified according to the manufacturer's protocol. Sequencing libraries were generated using the SeqPlex RNA Amplification Kit (Sigma) according to the manufacturer's instructions and sequenced to a depth of ~30 million raw reads per sample (single-end, 50 bp) on the Illumina HiSeq2500.

RNaseq alignment and DE analysis

Reads were mapped to the mouse genome mm10 using STAR. We used htseq to generate gene-count tables for all samples, then performed differential expression between the 3 replicates each from mock- or morphine-treated mice using DESeq. We first removed genes whose basemean expression was < 30, leaving ~12,000 genes. For Figure 4A, we filtered the genes by adjusted p value (p-adj) and $\log_2$(fold-change) to generate three lists with increasing stringency: "Top 1000" – p-adj < 0.05 and abs[$\log_2$FC] > 0.5; "Top 500" – p-adj < 1e-7 and abs[$\log_2$FC] > 0.5; "Top 200" – p-adj < 1e-12 and abs[$\log_2$FC] > 1. SCDE false discovery rate (FDR) was determined by dividing the number of true positives (which were defined as those present in the Top 1000 list) by the total number of genes at a given SCDE p value cutoff. FDR calculations were iterated over the full range of SCDE p value thresholds. An empirical FDR of ~3.5% corresponded to an SCDE p value cutoff of 0.13.

Pathway analysis of RNaseq data

Pathway analysis was performed using Genomatix GeneRanker software. For single-cell data, we used as input lists: (i) genes enriched in D1 MSNs of the activated MSN cluster compared to all other D1 MSNs (SCDE p < 0.001; 256 genes), (ii) morphine-regulated genes in OLs (SCDE p < 0.05, abs[$\log_2$FC] > 0.4; 69 genes), or (iii) morphine-regulated genes in astrocytes (SCDE p < 0.3; 81 genes). For bulk RNaseq analysis, we used the top 200 morphine-induced (p-adj < 1e-12, $\log_2$FC > 1) or the top 148 morphine-repressed (p-adj < 1e-8, $\log_2$FC < −0.5) genes.

QUANTIFICATION AND STATISTICAL ANALYSIS

Single-cell analysis

Error bars in Figures 2B, 4B, and S2 represent the standard deviation among four biological replicates per treatment.

FISH

Quantification in Figures 5 and S5 was performed using Fiji/ImageJ software (Schindelin et al., 2012). RGB channels corresponding to the two Affymetrix probes and DAPI were split. RNA particles in each channel were then identified in a semi-automated manner by selecting an intensity threshold above which a spot is considered an RNA particle. The number of puncta, their average size, and total area of signal was calculated for each probe. Cell number was quantified by DAPI signal using the NucleusCounter plugin in ImageJ. For Figure S5, positive cells were defined as having at least 5 puncta for the designated gene within 1 micron of the nucleus. For Figure 5, OLs were defined as having at least 2 *Mbp* puncta within 1 micron of the nucleus. By these criteria, ~95% of the cells in the anterior commissure and corpus callosum and ~10% of cells in the NAc were classified as OLs. Error bars represent the standard deviation among three biological replicates (3 mice per condition) and statistical significance was assessed by paired t test, two-sided.

qRT-PCR

Differences in relative gene expression were calculated using the delta delta cT method after normalization to beta-actin. Values shown are the mean plus SEM of three biological replicates (Figure S6) or three replicate plates (Figure S7), with each sample run in technical triplicate.

DATA AND SOFTWARE AVAILABILITY

The accession number for the raw and processed sequencing data reported in this paper is GEO: GSE118918.

Cell Reports, Volume *24*

Supplemental Information

Single-Cell RNA-Seq Uncovers a Robust Transcriptional Response to Morphine by Glia

Denis Avey, Sumithra Sankararaman, Aldrin K.Y. Yim, Ruteja Barve, Jeffrey Milbrandt, and Robi D. Mitra

A

Replicate	Treatment (# mice)	Age (Days ± SD)
1	Mock (2)	43.5 ± 2.1
	Morphine (2)	43.5 ± 2.1
2	Mock (2)	39.5 ± 3.5
	Morphine (2)	39 ± 2.1
3	Mock (2)	80 ± 2.8
	Morphine (2)	80 ± 2.8
4	Mock (2)	78 ± 0
	Morphine (2)	78 ± 0

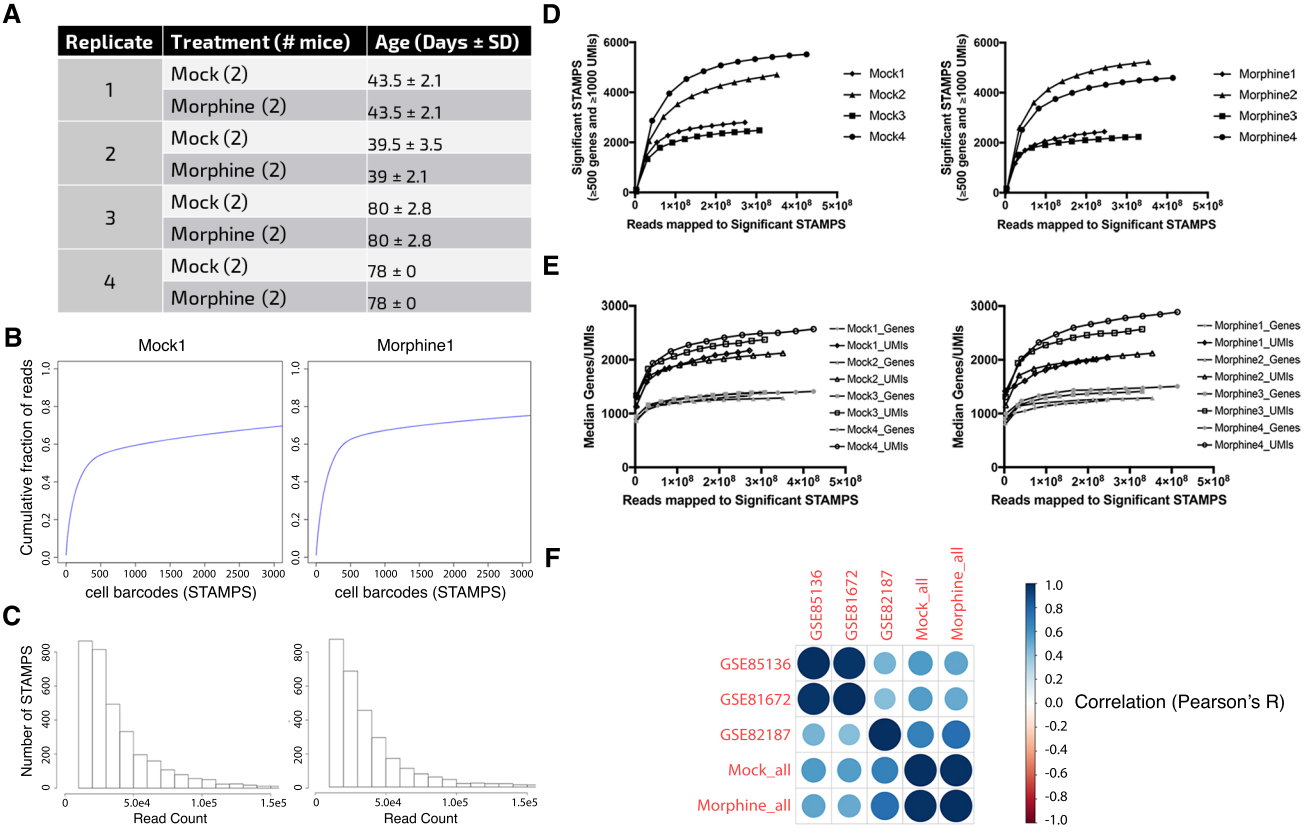

Figure S1. Quality control of Drop-seq libraries and correlation with previous RNA-seq datasets of the mouse nucleus accumbens, Related to Figure 1. (**A**) Age of mice for each biological replicate. (**B**) Cumulative read distribution for a subset of STAMPS (~500) from the first biological replicate. (**C**) Read count distribution for Mock1 and Morphine1. (**D-E**) Number of Significant STAMPS (**D**) or median genes and UMIs (**E**) were plotted for each sample as a function of sequencing depth. (**F**) Our samples (log-transformed gene expression averaged across all single cells) correlate well with three previously published gene expression datasets of the mouse nucleus accumbens.

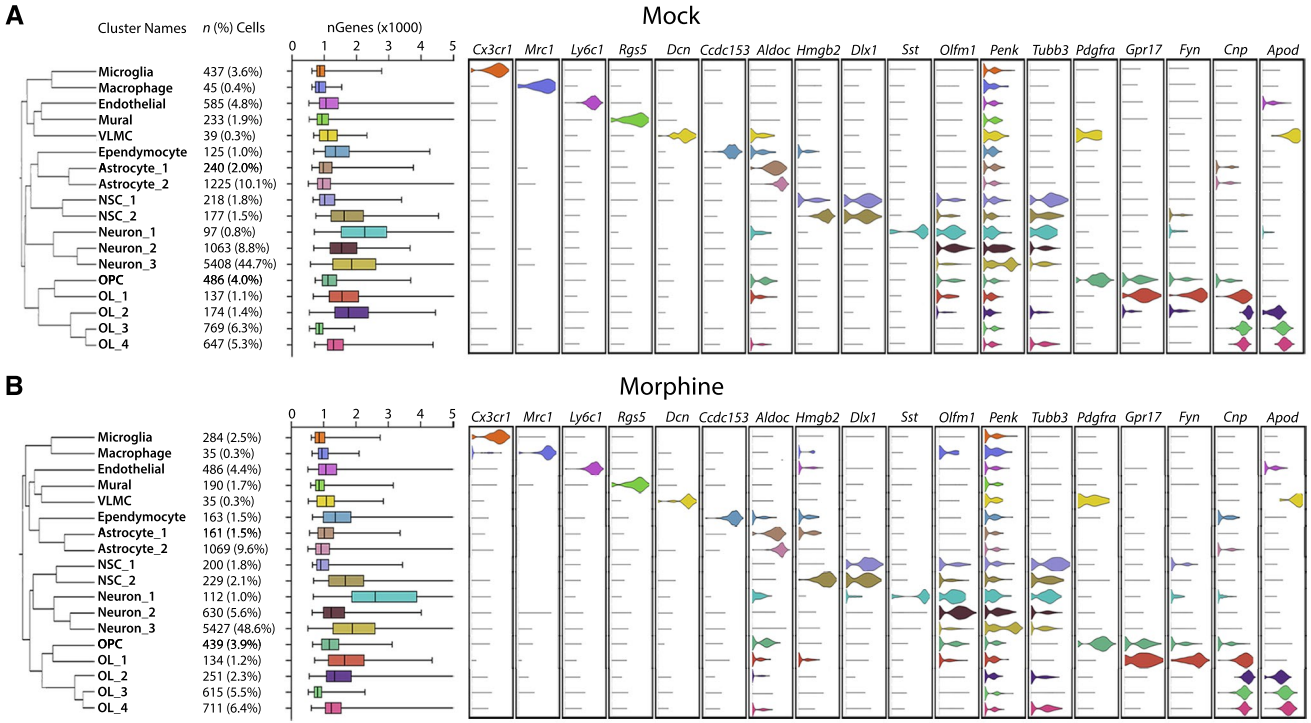

Figure S2. Proportions and marker genes of major CNS cell types are unchanged by acute morphine treatment, Related to Figure 1. On left, unbiased hierarchical clustering yields highly similar trees. The number (and percentage) of cells identified per cluster, number of genes (nGenes), and expression of cell type marker genes are also comparable between mock and morphine samples (clusters are color-coordinated as in Figure 1). In the nGenes box-and-whisker plots, the vertical line represents the median across all single cells in a given cluster, the box extends from the 25th to 75th percentile, and the whiskers extend from the minimum to maximum. Those with an open-ended whisker have a max number of genes greater than 5000.

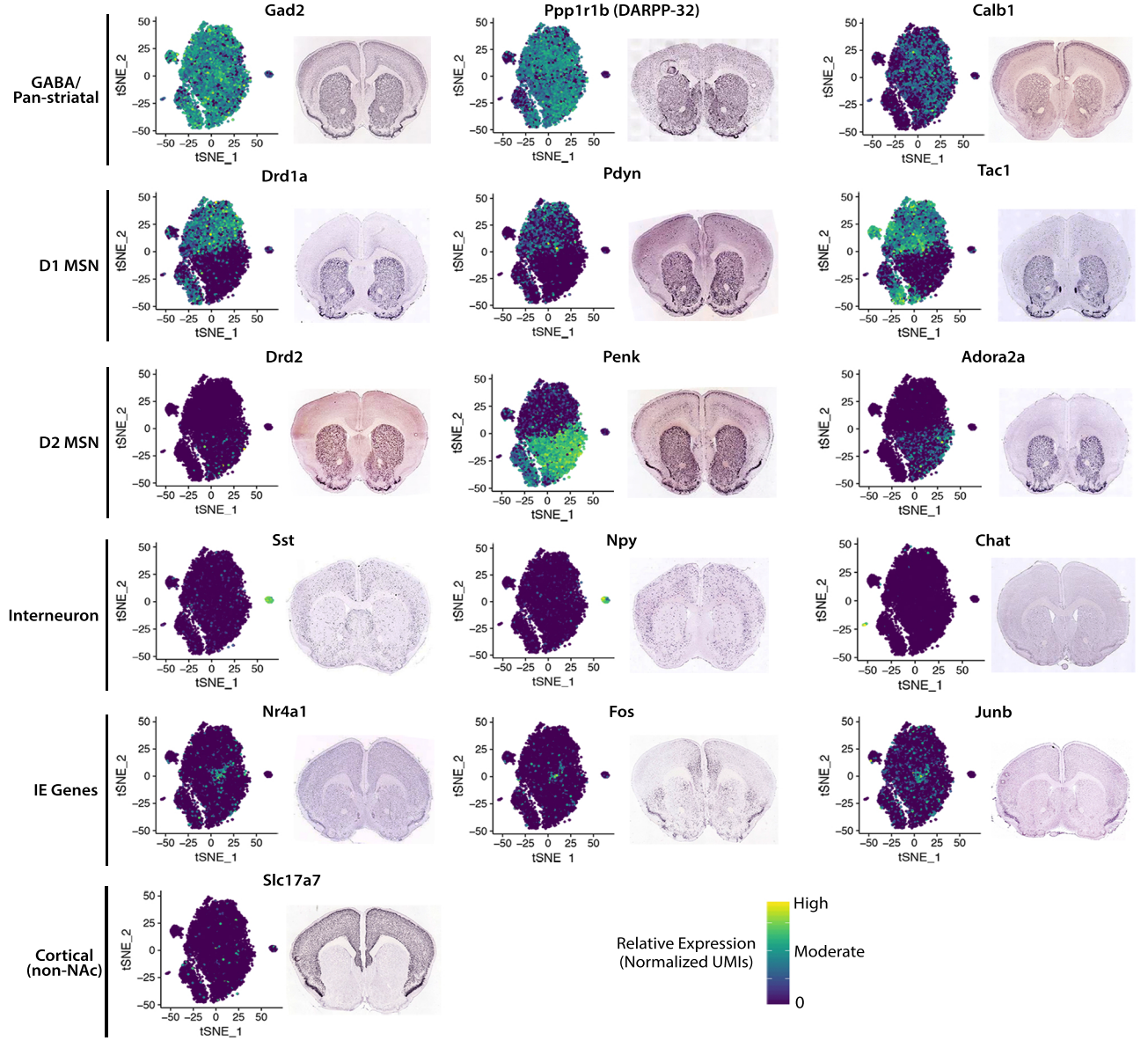

Figure S3. Neuronal subcluster-enriched genes are expressed in the nucleus accumbens, Related to Figure 2. t-SNE plots of neuron subclusters were overlaid with single-cell expression of cluster-enriched marker genes, which correlates well with published ISH data (at Bregma +1; Allen Brain Atlas).

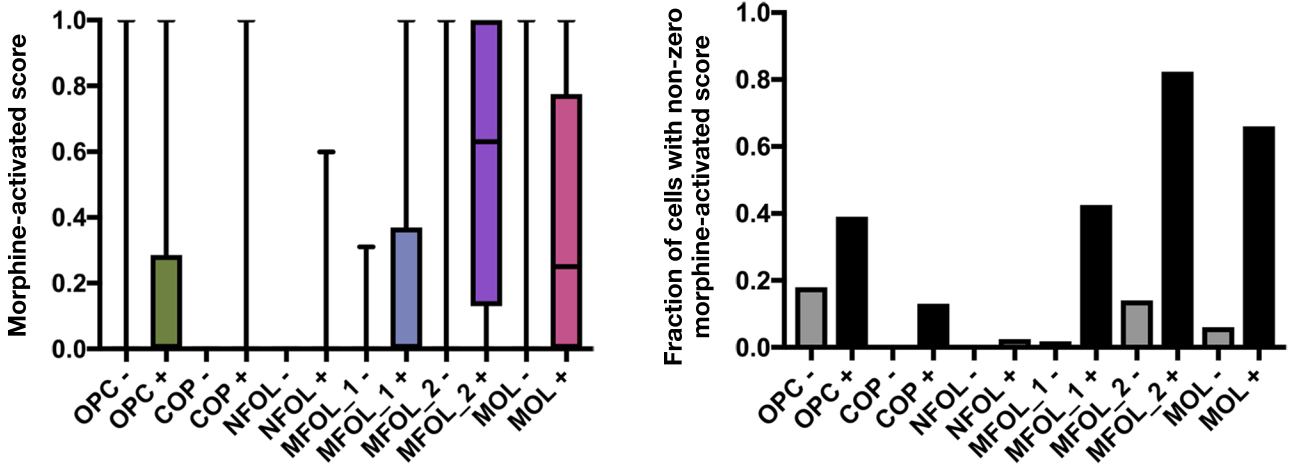

Figure S4. Morphine-activated score for oligodendrocyte subclusters, Related to Figure 4. A morphine-activated score was generated for each cell from the OL lineage (see Methods). (left panel) The distribution of scores is plotted for cells from each oligodendrocyte subcluster from mock (-) or morphine (+) treated mice. Horizantal lines, box boundaries, and error bars denote median, 25th/75th percentile, and min/max, respectively. (right panel) The fraction of cells from each cluster with a non-zero morphine-activated score is plotted. OPC: OL progenitor cell; COP: differentiation-committed OL progenitor; NFOL: newly formed OL; MFOL: myelin-forming OL; MOL: mature OL.

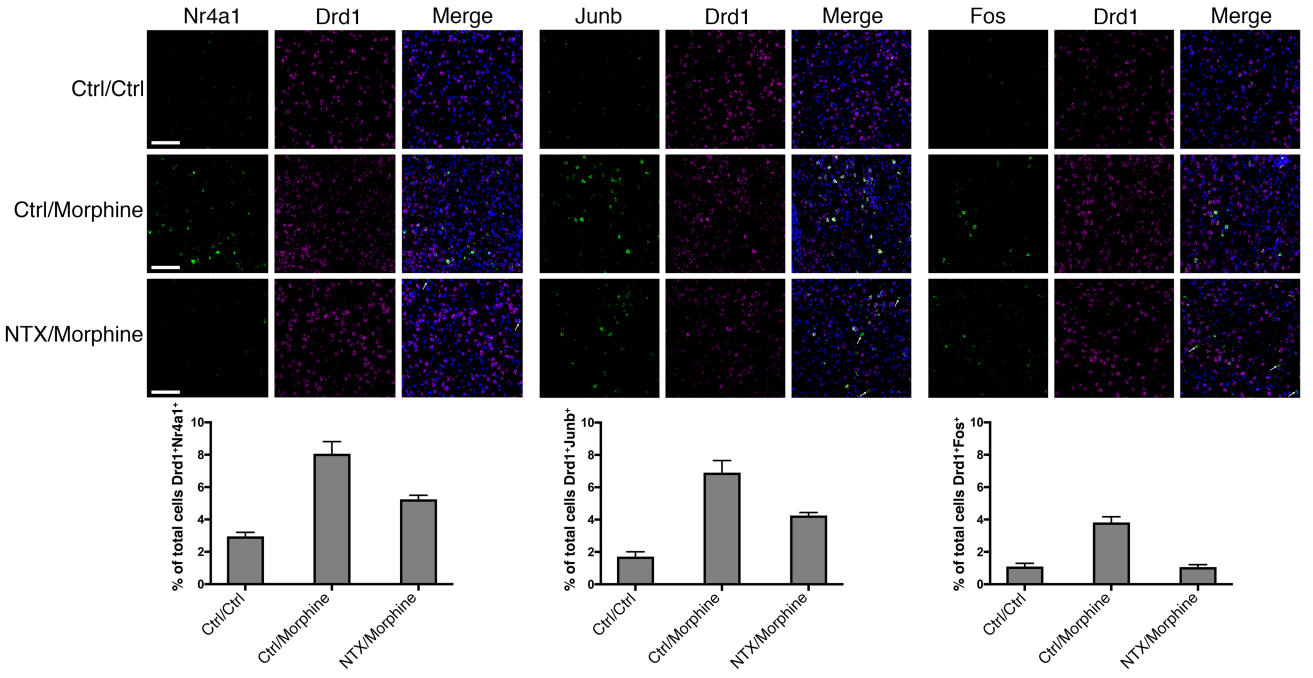

Figure S5. Morphine induces the expression of immediate-early genes (IEGs) in the nucleus accumbens in an opioid receptor-dependent manner, Related to Figure 5. Arrows in NTX/Morphine Merge panels indicate cells positive for the indicated IEG (*Nr4a1*, *Junb*, or *Fos*), but negative for *Drd1*. Quantification is shown as percentage of total cells in the nucleus accumbens that are double-positive for *Drd1* and the designated IEG. Error bars are the standard deviation among three biological replicates (n=1000 cells per probe pair per replicate). NTX: Naltrexone.

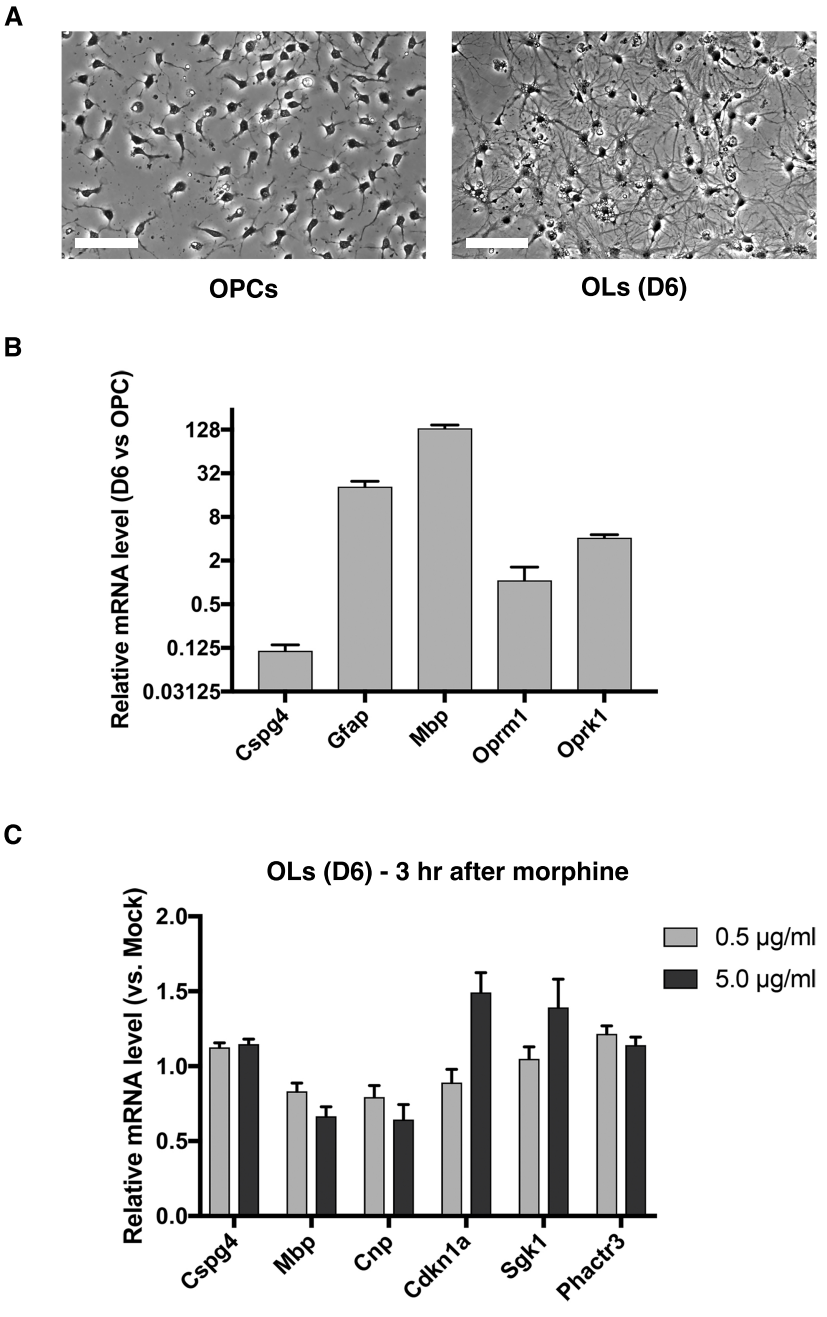

Figure S6. ***In vitro*** **OL culture failed to recapitulate morphine-dependent changes observed** ***in vivo*****, Related to Figures 4 and 5.** (**A**) Bright-field micrographs of purified OPCs (2 days after isolation and plating) and OLs (D4: 4 days of differentiation). Scale bar = 100 µm. (**B**) qRT-PCR of the indicated genes comparing relative expression between OLs (6 days of differentiation) and OPCs. (**C**) qRT-PCR of the indicated genes following a 3-hour treatment of D6 OLs with morphine. In (**B**) and (**C**), values were normalized to *Gapdh*, and error bars represent the standard deviation among three biological replicates.

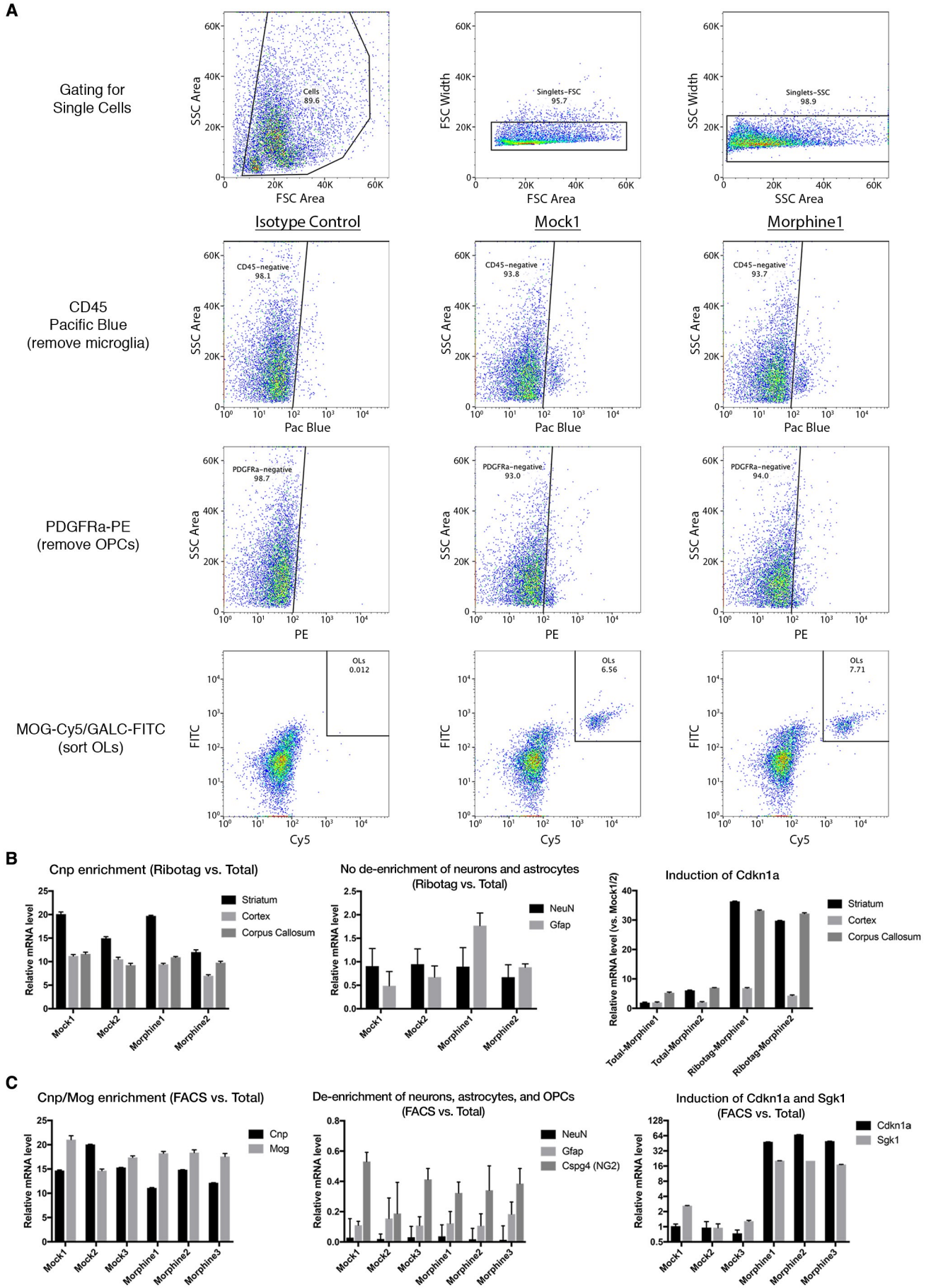

Figure S7. Representative FACS plots illustrating strategy to purify OLs, and qRT-PCR validating enrichment, Related to Figure 6. (**A**) Immunostaining and FACS were performed to obtain GALC^{+}/MOG^{+} oligodendrocytes from whole brains of adult mice (mock- or morphine-treated). (**B and C**) qRT-PCR results showing relative enrichment of OL-specific genes (left panel), de-enrichment of other cell type markers (middle panel), and expression of morphine-induced genes (right panel) using oligodendrocyte RNA isolated from (**B**) Cnp-Cre Ribotag mice or (**C**) the FACS strategy outlined in (**A**). We chose to proceed with FACS rather than Ribotag because of the dramatically improved de-enrichment of neuronal (*NeuN*) and astrocytic (*Gfap*) mRNAs. Error bars represent the SEM among nine technical replicates.

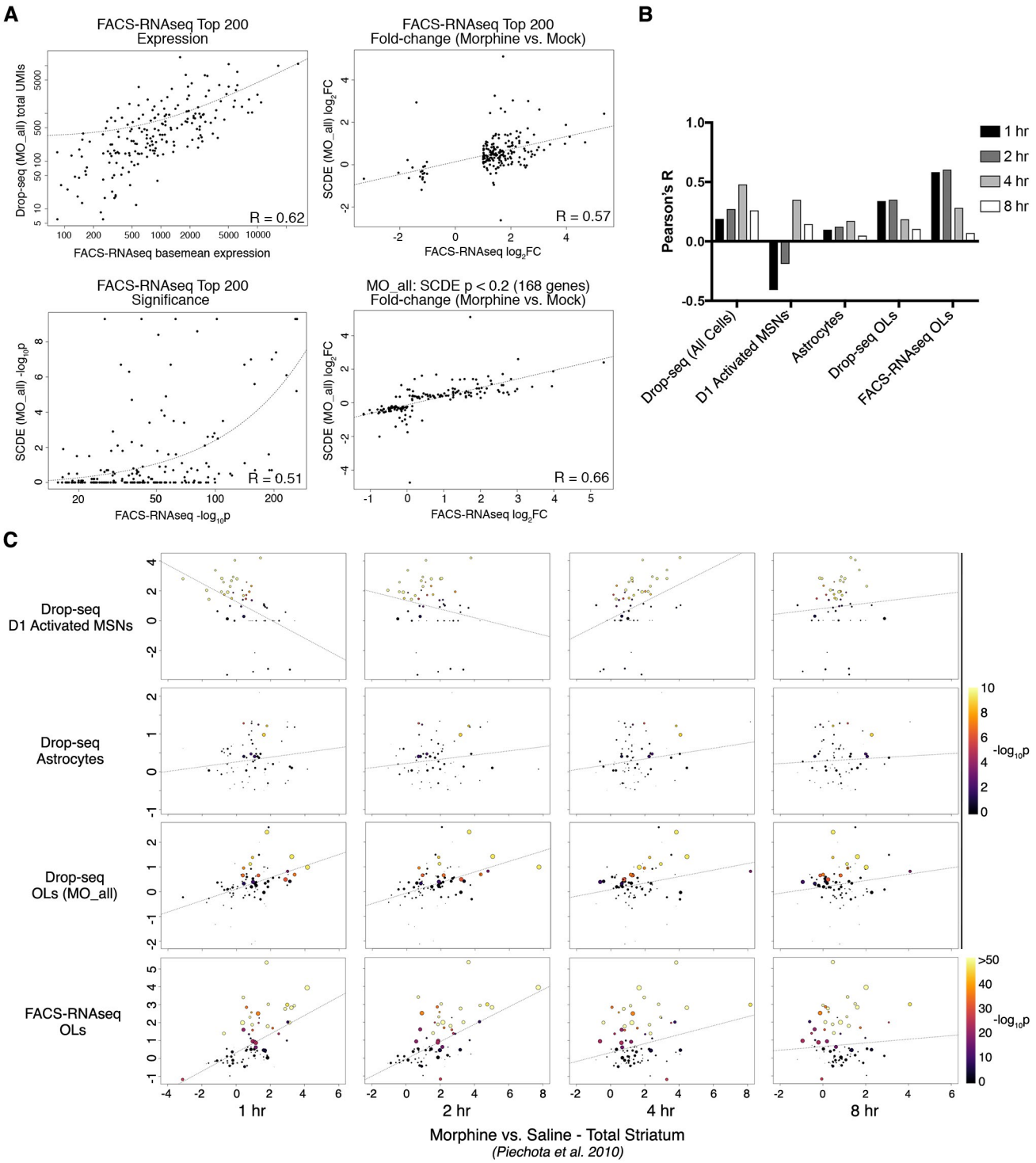

Figure S8. Correlation analyses between single-cell, FACS-RNAseq, and published microarray data, Related to Figure 6. (**A**) Log_2FC correlation plot of OL-specific morphine-regulated genes as assessed by Drop-seq/SCDE (y-axis) or FACS-RNASeq/DESeq ("Top 200"; x-axis). (**B**) Correlation values (Pearson's R) for each pair-wise comparison in (C). (**C**) Log_2FC correlation plots comparing the expression of previously identified morphine-regulated genes at various timepoints (1, 2, 4, or 8 hours; Piechota *et al.*, 2010; x-axis) with their expression in neurons (D1 Activated MSNs: Activated MSNs expressing *Drd1a*), astrocytes, or oligodendrocytes. Points are colored by $-log_{10}(p)$ and sized by their relative expression in our data (larger points denote higher expression). The different patterns observed for distinct cell types suggests temporal differences in their responsiveness to morphine exposure.

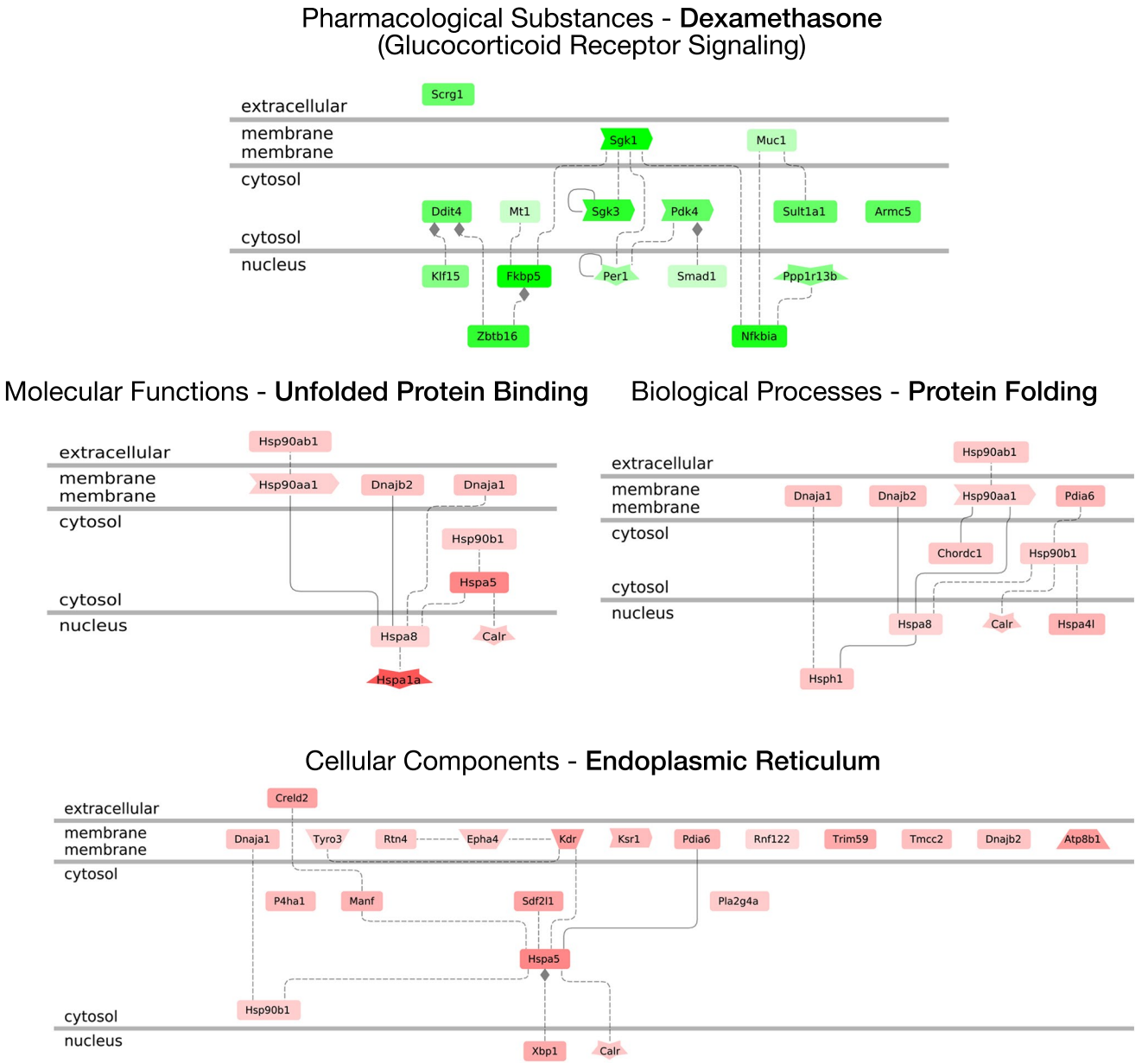

Figure S9. Summary of the most significantly enriched biological pathways and terms among morphine-regulated genes in oligodendrocytes, Related to Figures 6 and 7. These terms are significantly enriched as assessed by GeneRanker software (see also Table S3). Genes are arranged by their reported subcellular localization and interactions and colored by the magnitude of $\log_2$FC (green – upregulated by morphine; red – downregulated by morphine). Dexamethasone p = 5.32e-4; Unfolded Protein Binding p = 1.27e-9; Protein Folding p = 2.43e-9; Endoplasmic Reticulum p = 3.5e-4. Adjustped p-values for these terms are < 0.001 for all.